

New Class of Homoleptic and Heteroleptic Bis(terpyridine) Iridium(III) Complexes with Strong Photodynamic Therapy Effects

Bingqing Liu,[†] Susan Monro,[‡] Zhike Li,[§] Mohammed A. Javed,[†] Daniel Ramirez,[†] Colin G. Cameron,^{||} Katsuya Colón,^{||} John Roque, III,^{||} Svetlana Kilina,[†] Jian Tian,^{*,§} Sherri A. McFarland,^{*,‡,||} and Wenfang Sun^{*,†}

[†]Department of Chemistry and Biochemistry, North Dakota State University, Fargo, North Dakota 58108-6050, United States

[‡]Department of Chemistry, Acadia University, 6 University Avenue, Wolfville, NS B4P 2R6, Canada

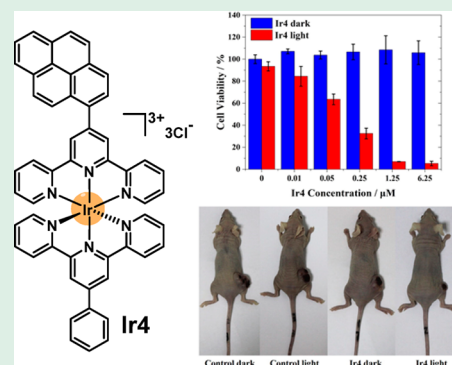
[§]Key Laboratory of Combinatorial Biosynthesis and Drug Discovery (MOE), Hubei Province Engineering and Technology Research Center for Fluorinated Pharmaceuticals, School of Pharmaceutical Sciences, Wuhan University, Wuhan 430071, P. R. China

^{||}Department of Chemistry and Biochemistry, University of North Carolina at Greensboro, Greensboro, North Carolina 27402-6170, United States

Supporting Information

ABSTRACT: Six homo- or heteroleptic tricationic Ir(R₁-tpy)(R₂-tpy)³⁺ complexes (Ir1–Ir6, R₁/R₂ = Ph, 4'-N(CH₃)₂Ph, pyren-1-yl, or 4'-{2-[2-(2-methoxyethoxy)ethoxy]ethoxy}Ph, tpy = 2,2',6',2''-terpyridine) were synthesized and tested for photodynamic therapy (PDT) effects. The ground- and excited-state characteristics of these complexes were studied systematically via spectroscopic methods and quantum chemistry calculations. All complexes possessed intraligand charge transfer (¹ILCT)/metal-to-ligand charge transfer (¹MLCT) dominated transition(s) in their low-energy absorption bands, which red-shifted with the increased electron-releasing strength of the R₁/R₂ substituent. Five of the complexes exhibited ligand-centered ³π,π*/³ILCT/³MLCT emission. With a stronger electron-releasing R₁/R₂ substituent, the degree of charge-transfer contribution increased, leading to a decrease of the emission quantum yield. When the 4'-N(CH₃)₂Ph substituent was introduced on both tpy ligands, the emission of Ir3 was completely quenched. Our study on the transient absorption of these complexes demonstrated that they all possessed broadband triplet excited-state absorption in the visible to the near-IR regions. Pyrenyl substitution of one or both tpy ligands, as in Ir4 and Ir5, increased the lifetimes of the lowest triplet excited state and the singlet oxygen (¹O₂) production efficiencies. Ir1–Ir5 were nontoxic toward SK-MEL-28 cells, with photocytotoxicities that varied from 0.18 to 153 μM (EC₅₀ values). Among them, Ir4 had the highest ¹O₂ quantum yield (0.81) in cell-free conditions, showing the largest photocytotoxicity against SK-MEL-28 cells for Ir(III) PSs to date, and was the most efficient generator of reactive oxygen species (ROS) *in vitro*. Ir4 possessed a very large phototherapeutic index (PI = dark EC₅₀/light EC₅₀) of >1657, the largest reported for an Ir(III) complex photosensitizer upon broadband visible light (400–700 nm) activation. Ir4 also exhibited a very strong PDT effect toward MCF-7 breast cancer cells and its xenograft tumor model. Upon 450 nm light activation, Ir4 dramatically inhibited the xenograft tumor growth and exhibited negligible side effects upon PDT treatment.

KEYWORDS: bis(terpyridine) iridium(III) complex, photophysics, photodynamic therapy, photobiological activity, reactive oxygen species, absorption, emission, transient absorption



INTRODUCTION

Photodynamic therapy (PDT), a noninvasive and spatiotemporally selective anticancer strategy, has attracted continued interest over the past few decades.^{1,2} PDT depends on the interaction of a photosensitizer (PS) and oxygen upon light activation to generate cytotoxic singlet oxygen (¹O₂) via energy transfer (type II) or other reactive oxygen species (ROS) via electron transfer (type I), from the excited triplet state of a photosensitizer (PS).³ The sensitized ¹O₂ and/or other ROS species irreversibly damage(s) tumor cells, tumor vasculature,

and have/has the capacity to invoke an antitumor immune response. Because the PS plays a critical role in PDT, the search for better PSs with effective ¹O₂ and/or ROS generation is an active area of investigation.^{4,5}

Porphyrin-based compounds have been widely studied PSs for PDT,^{6–9} but the only FDA-approved clinical PS for cancer

Received: April 12, 2019

Accepted: June 18, 2019

Published: June 18, 2019



therapy is Photofrin. Despite its prolific use in the field of PDT, there has been ongoing interest in the development of new PSs with better, or simply different, properties.^{10–15} Transition metal complexes in particular have emerged as promising candidates.^{5,16–19} In comparison to the porphyrin PSs and other organic PSs, transition metal complex PSs possess some unique merits, such as (i) the ability to tune the singlet and triplet excited-state properties independently,^{2,5,20} (ii) very high triplet excited-state quantum yields, (iii) the opportunity to select coordinating ligands for better thermal and kinetic stability, and (iv) the existence of a number of excited-state configurations that can be accessed with visible light.¹⁸ Additionally, many transition metal complexes, such as the Ru(II) and Ir(III) complexes in particular, exhibit bright red to near-infrared phosphorescence for *in situ* monitoring of PS distribution in tumors and cells, providing novel theranostic platforms for imaging-guided PDT and aiding in the mechanistic study of PDT in order to optimize the treatment efficacy.^{11,21–27}

Among the variety of transition metal complexes, cationic Ir(III) complexes, with octahedral d^6 geometry, appear promising as theranostic PDT agents due to their high quantum yields for triplet excited-state formation and long triplet excited-state lifetimes. Together, these facilitate efficient 1O_2 generation through type II energy transfer with bright intracellular luminescence for imaging.^{11,19–27} While Ir(III) is able to form complexes with coordinating or cyclometalating bidentate or terdentate ligands,^{11,19–38} only the tris-bidentate Ir(III) complexes featuring various diimine, cyclometalating, or dianionic ligands have been widely studied for theranostic PDT applications.^{11,19–36} Investigations of bisterdentate Ir(III) complexes for PDT are relatively scarce.³⁹

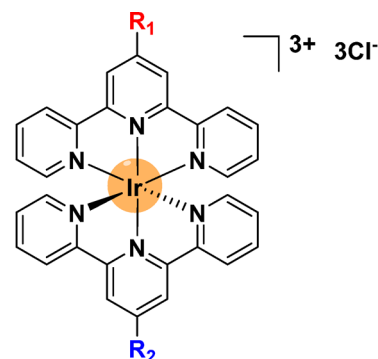
The bis(terpyridine) (tpy) coordinated Ir(III) complexes are less studied, in part, due to the harsh reaction conditions required for synthesizing them. However, this arrangement has the advantage of higher geometric symmetry, precluding the formation of stereoisomers. The higher 3+ charge of Ir (versus Ru^{2+}) may improve the solubility of these complexes in water. Among the reported mono- or multinuclear $Ir(ph-tpy)_2^{3+}$ -based complexes,^{40–44} some were demonstrated to exhibit aqueous solubility⁴¹ and have long-lived triplet excited states,⁴⁰ which are desirable features for PSs. However, the exploration of these Ir(III) bis(terpyridine) complexes for biological applications is undeveloped.^{39,43,45,46}

To the best of our knowledge, the only report on bisterdentate Ir(III) complexes for PDT is a series of dinuclear Ir(III) complexes with fluorenyl-linked ditopic terpyridine as the bridging ligand and various terdentate ligands as the end-capped ligands, which was reported by us.³⁹ We demonstrated that these complexes could be used as *in vitro* PDT agents toward human SK-MEL-28 melanoma cells when activated with visible light. They possessed submicromolar photocytotoxicity, and the phototherapeutic indices (PIs) were 20–288. All of the complexes were brightly phosphoresced when entered compromised cells and light irradiation enhanced the cellular uptake. These features highlighted the theranostic potential of this new class of Ir(III) complex PSs. We also found that variation of the terminal terdentate ligands drastically altered the photophysical properties and consequently the *in vitro* PDT effects.

Inspired by the aforementioned results, herein we further explore Ir(III) bis(terpyridine) complexes for PDT applications with a focus on the mononuclear $Ir(R-tpy)_2^{3+}$ scaffold

with different substituents on the tpy ligands. Six hetero- or homoleptic $Ir(R_1-tpy)(R_2-tpy)^{3+}$ complexes (**Ir1–Ir6** in Chart 1) were synthesized and fully characterized and investigated for

Chart 1. Structures of Homo- and Heteroleptic Ir(III) Bis(terpyridine) Complexes Ir1–Ir6



- Ir1:** $R_1 = R_2 = Ph$
Ir2: $R_1 = 4'-N(CH_3)_2Ph$, $R_2 = Ph$
Ir3: $R_1 = R_2 = 4'-N(CH_3)_2Ph$
Ir4: $R_1 = Pyren-1-yl$, $R_2 = Ph$
Ir5: $R_1 = R_2 = Pyren-1-yl$
Ir6: $R_1 = 4'-CH_3(OCH_2CH_2)_3OPh$, $R_2 = Ph$

their potential as PDT agents. Different 4'-substituted phenyl or pyren-1-yl groups were introduced to the tpy ligand(s) in order to tune the photophysical properties and photobiological activities of this class of Ir(III) PSs. Dimethylaminophenyl and pyren-1-yl substituents were introduced to the tpy ligand(s) to probe the effect of an increase in the intraligand charge-transfer (ILCT) character of the excited state, while the 2-[2-(2-methoxyethoxy)ethoxy]ethoxy substituent was appended to one of the phenyl groups to enhance water solubility, which can be visualized by the naked eye.

EXPERIMENTAL SECTION

Synthesis and Characterization. All reagents used in this work were purchased from Sigma-Aldrich or Alfa Aesar and used as received without any further purification. The Al_2O_3 (activated, neutral) and silica (60 Å, 230–400 mesh) gels used for column chromatography were obtained from Sorbent Technology. The 4-substituted tpy ligands, i.e., 4-phenyltpy, 4-(4'-dimethylaminophenyl)tpy, and 4-(pyren-1-yl)tpy, were synthesized from 2-acetylpyridine and the corresponding 4-substituted benzaldehyde according to the published procedures.^{47–49} Compound 4-{2-[2-(2-methoxyethoxy)ethoxy]ethoxy}benzaldehyde was synthesized from 2-[2-(2-methoxyethoxy)ethoxy]ethanol and 4-methylbenzenesulfonyl chloride, followed by a reaction with 4-hydroxybenzaldehyde according to the reported method.⁵⁰ Complex 4-Ph-tpy- $IrCl_3$ was prepared based on the literature procedure.⁵¹ The synthesized complexes **Ir1–Ir6** were characterized by 1H NMR, high-resolution electrospray ionization mass spectrometry (ESI-MS), and elemental analysis. 1H NMR spectra were recorded on Bruker-400 or Varian Oxford-VNMR (500 MHz) spectrometers. ESI-MS analyses were conducted on a Bruker BioTOF III mass spectrometer. Elemental analyses were carried out by NuMega Resonance Laboratories, Inc., in San Diego, California.

4-{4'-[2-[2-(2-Methoxyethoxy)ethoxy]ethoxy]phenyl}tpy. 2-Acetylpyridine (2.42 g, 20 mmol), 4-{2-[2-(2-methoxyethoxy)ethoxy]ethoxy}benzaldehyde (2.68 g, 10 mmol), and KOH (1.12 g, 20 mmol) were added to EtOH solution. Then the mixture reacted at room temperature for 2 h under stirring. After that, ammonium hydroxide (20 mL, 28% NH_3 aqueous solution) was added into the

mixture, and the solution was brought to reflux for 24 h. After cooling to room temperature, the solution was poured to water, and then the crude product was extracted by dichloromethane. After drying the dichloromethane layer and removing the solvent, the crude product was separated on a silica gel column eluted with ethyl acetate/hexane (1:1, v/v) to obtain a yellow oil as the target compound (1.51 g, 32%). ¹H NMR (500 MHz, CDCl₃): δ 8.76–8.72 (m, 2H), 8.71 (s, 2H), 8.67 (dd, *J* = 7.9, 0.8 Hz, 2H), 7.87 (d, *J* = 8.7 Hz, 4H), 7.38–7.32 (m, 2H), 7.05 (d, *J* = 8.5 Hz, 2H), 4.24–4.18 (m, 2H), 3.94–3.89 (m, 2H), 3.77 (dd, *J* = 5.7, 3.9 Hz, 2H), 3.71 (dd, *J* = 5.5, 3.8 Hz, 2H), 3.69–3.65 (m, 2H), 3.57 (dd, *J* = 5.5, 3.7 Hz, 2H), 3.39 (s, 3H).

General Synthetic Procedure for 4-R-tpy-IrCl₃. A degassed ethylene glycol suspension of the corresponding 4-R-tpy (0.1 mmol, R = 4'-dimethylaminophenyl or pyren-1-yl) and IrCl₃·H₂O (0.1 mmol) was heated to 160 °C in the dark. After 15 min, the mixture was cooled to room temperature. The formed precipitate was filtered out and washed with water (10 mL × 2) and ethanol (10 mL × 2) and dried in vacuum. The obtained solid was then used for the next step reaction without further purification.

4-(4'-Dimethylaminophenyl)tpy-IrCl₃. A dark red powder was obtained as the product (41 mg, 63%). ¹H NMR (400 MHz, DMSO): δ 9.21 (dd, *J* = 5.6, 1.0 Hz, 2H), 8.97 (s, 2H), 8.89 (d, *J* = 8.1 Hz, 2H), 8.27 (td, *J* = 7.9, 1.5 Hz, 2H), 8.13 (d, *J* = 9.0 Hz, 2H), 7.97–7.89 (m, 2H), 6.93 (d, *J* = 9.1 Hz, 2H), 3.10 (s, 6H).

4-(Pyren-1-yl)tpy-IrCl₃. A yellow powder was obtained as the product (50 mg, 68%). ¹H NMR (400 MHz, DMSO): δ 9.27 (dd, *J* = 5.6, 1.0 Hz, 2H), 9.11 (s, 2H), 8.82 (d, *J* = 8.1 Hz, 2H), 8.56 (d, *J* = 8.0 Hz, 1H), 8.45–8.32 (m, 7H), 8.26 (td, *J* = 7.9, 1.6 Hz, 2H), 8.18 (t, *J* = 7.6 Hz, 1H), 8.02–7.97 (m, 2H).

General Synthetic Procedure for Complexes Ir1–Ir6. A degassed ethylene glycol suspension of 4-R-tpy-IrCl₃ (0.1 mmol) (R = phenyl for Ir1, Ir2, Ir4, and Ir6; 4'-dimethylaminophenyl for Ir3; and pyren-1-yl for Ir5) and the other corresponding tpy-based ligand (0.1 mmol) was heated to 196 °C in the dark for 1 h. After the mixture was cooled to room temperature, 10 mL of aqueous NH₄PF₆ (0.3 mmol) was added to precipitate out the crude product. The crude product was then purified by column chromatography on alumina gel. Dichloromethane and hexane (1:1, v/v) were used as the eluent first to remove the unreacted tpy ligands. Then, the mixed acetone/water eluent was used with a gradient of 100:0 to 95:5 (v/v) to obtain the target complexes.

Ir1. A yellow powder was obtained as the product (80 mg, 64%). ¹H NMR (400 MHz, DMSO): δ 9.62 (s, 4H), 9.22 (d, *J* = 8.1 Hz, 4H), 8.52–8.41 (m, 4H), 8.38 (td, *J* = 8.0, 1.4 Hz, 4H), 7.95 (d, *J* = 4.9 Hz, 4H), 7.85 (t, *J* = 7.6 Hz, 4H), 7.76 (t, *J* = 7.4 Hz, 2H), 7.62–7.52 (m, 4H). ESI-HRMS (*m/z*, in acetonitrile): calcd for [C₄₂H₃₀IrN₆]³⁺, 270.4055; found, 270.4060. Anal. Calcd (%) for C₄₂H₃₀F₁₈IrN₆P₃·0.8H₂O: C, 40.03; H, 2.53; N, 6.67. Found: C, 40.39; H, 2.93; N, 7.06.

Ir2. A red powder was obtained as the product (28 mg, 22%). ¹H NMR (500 MHz, DMSO): δ 9.60 (s, 2H), 9.44 (s, 2H), 9.20 (dd, *J* = 7.7, 4.5 Hz, 4H), 8.43 (t, *J* = 8.7 Hz, 4H), 8.35 (dd, *J* = 16.3, 8.2 Hz, 4H), 7.98 (d, *J* = 5.9 Hz, 2H), 7.92 (d, *J* = 5.9 Hz, 2H), 7.84 (t, *J* = 7.6 Hz, 2H), 7.76 (t, *J* = 7.4 Hz, 1H), 7.62–7.56 (m, 2H), 7.53 (t, *J* = 6.5 Hz, 2H), 7.03 (d, *J* = 8.9 Hz, 2H), 3.18 (s, 6H). ESI-HRMS (*m/z*, in acetonitrile): calcd for [C₄₄H₃₅IrN₇]³⁺, 284.7529; found, 284.7528. Anal. Calcd (%) for C₄₄H₃₅F₁₈IrN₇P₃: C, 41.00; H, 2.74; N, 7.61. Found: C, 40.64; H, 2.58; N, 7.61.

Ir3. A red powder was obtained as the product (61 mg, 46%). ¹H NMR (400 MHz, DMSO): δ 9.42 (s, 4H), 9.18 (d, *J* = 8.2 Hz, 4H), 8.41 (d, *J* = 9.2 Hz, 4H), 8.33 (td, *J* = 8.0, 1.4 Hz, 4H), 7.98–7.91 (m, 4H), 7.58–7.47 (m, 4H), 7.03 (d, *J* = 9.2 Hz, 4H), 3.18 (s, 12H). ESI-HRMS (*m/z*, in acetonitrile): calcd for [C₄₆H₄₀IrN₈]³⁺, 299.1003; found, 299.1010. Anal. Calcd (%) for C₄₆H₄₀F₁₈IrN₈P₃·4H₂O: C, 39.35; H, 3.45; N, 7.98. Found: C, 39.33; H, 3.48; N, 8.05.

Ir4. A red powder was obtained as the product (118 mg, 86%). ¹H NMR (400 MHz, DMSO): δ 9.68 (s, 2H), 9.65 (s, 2H), 9.30 (d, *J* = 8.2 Hz, 2H), 9.14 (d, *J* = 8.0 Hz, 2H), 8.73 (dd, *J* = 14.2, 8.6 Hz, 2H), 8.54–8.49 (m, 5H), 8.48–8.41 (m, 4H), 8.33 (dd, *J* = 12.6, 4.6 Hz, 2H), 8.26 (t, *J* = 7.6 Hz, 2H), 8.16 (d, *J* = 5.2 Hz, 2H), 8.02 (d, *J* = 5.7

Hz, 2H), 7.87 (t, *J* = 7.5 Hz, 2H), 7.78 (t, *J* = 7.4 Hz, 1H), 7.73–7.68 (m, 2H), 7.60 (dd, *J* = 10.5, 4.3 Hz, 2H). ESI-HRMS (*m/z*, in acetonitrile): calcd for [C₅₂H₃₄IrN₆]³⁺, 311.7493; found, 311.7489. Anal. Calcd (%) for C₅₂H₃₄F₁₈IrN₆P₃·1.2H₂O·0.6C₃H₆O (C₃H₆O: acetone): C, 45.30; H, 2.83; N, 5.89. Found: C, 45.52; H, 3.13; N, 6.14.

Ir5. A red powder was obtained as the product (107 mg, 71%). ¹H NMR (400 MHz, DMSO): δ 9.69 (s, 4H), 9.21 (d, *J* = 8.6 Hz, 4H), 8.80 (d, *J* = 9.4 Hz, 2H), 8.71 (d, *J* = 7.8 Hz, 2H), 8.60–8.57 (m, 2H), 8.50 (td, *J* = 12.1, 5.3 Hz, 10H), 8.42–8.35 (m, 6H), 8.25 (t, *J* = 7.7 Hz, 4H), 7.76–7.65 (m, 4H). ESI-HRMS (*m/z*, in acetonitrile): calcd for [C₆₂H₃₈IrN₆]³⁺, 353.0931; found, 353.0924. Anal. Calcd (%) for C₆₂H₃₈F₁₈IrN₆P₃·3H₂O·0.5C₆H₁₄ (C₆H₁₄: hexane): C, 49.06; H, 3.23; N, 5.28. Found: C, 48.69; H, 3.50; N, 5.49.

Ir6. A yellow powder was obtained as the product (74 mg, 53%). ¹H NMR (400 MHz, DMSO): δ 9.62 (s, 2H), 9.57 (s, 2H), 9.22 (d, *J* = 8.3 Hz, 4H), 8.49 (d, *J* = 8.9 Hz, 2H), 8.45 (d, *J* = 7.4 Hz, 2H), 8.37 (t, *J* = 7.9 Hz, 4H), 8.02–7.90 (m, 4H), 7.85 (t, *J* = 7.6 Hz, 2H), 7.77 (t, *J* = 7.4 Hz, 1H), 7.57 (dd, *J* = 12.1, 4.5 Hz, 4H), 7.41 (d, *J* = 8.9 Hz, 2H), 4.50 (s, 3H), 4.35–4.32 (m, 2H), 3.88–3.85 (m, 2H), 3.69–3.66 (m, 2H), 3.62–3.58 (m, 2H), 3.58–3.55 (m, 2H), 3.49–3.46 (m, 2H). ESI-HRMS (*m/z*, in acetonitrile): calcd for [C₄₉H₄₄IrN₆O₄]³⁺, 324.4352; found, 324.4362. Anal. Calcd (%) for C₄₉H₄₄F₁₈IrN₆O₄P₃·4H₂O·2C₃H₆O·1.5CH₂Cl₂ (C₃H₆O: acetone): C, 39.37; H, 3.92; N, 4.88. Found: C, 39.63; H, 3.92; N, 4.59. The solubility of this complex in H₂O is approximately 0.33 mg/mL.

Photophysical Measurements. The spectroscopic grade solvents used for the photophysical studies were purchased from Alfa Aesar. The UV–vis absorption spectra of complexes Ir1–Ir6 were recorded on a Varian Cary 50 spectrophotometer, and the steady-state emission spectra were measured using a HORIBA FluoroMax-4 fluorometer/phosphorometer. The relative actinometry method was applied for determining the emission quantum yields for all complexes. Quinine bisulfate ($\lambda_{\text{ex}} = 347.5 \text{ nm}$, $\Phi_{\text{em}} = 0.546$)⁵² in 1 N H₂SO₄ solution was used as the reference for complex Ir1, and the degassed acetonitrile solution of [Ru(bpy)₃]Cl₂ ($\Phi_{\text{em}} = 0.097$, $\lambda_{\text{ex}} = 436 \text{ nm}$)⁵³ was used as the reference for complexes Ir2–Ir6. For all of the emission measurements, the sample solutions were degassed with N₂ for 40 min prior to each measurement.

The nanosecond transient difference absorption (TA) measurements for complexes Ir1–Ir6 in degassed acetonitrile solutions were carried out on an Edinburgh LP920 laser flash photolysis spectrometer. The third harmonic output (355 nm) from a Quantel Brilliant Nd:YAG laser (pulse duration = 4.1 ns; repetition rate = 1 Hz) was used as the excitation light. The singlet depletion method⁵⁴ was used for determining the triplet excited-state molar extinction coefficients (ϵ_{T}). Then, the relative actinometry⁵⁵ was applied for calculating the triplet excited-state quantum yields, with SiNC in benzene solution ($\epsilon_{590 \text{ nm}} = 70 \text{ 000 L mol}^{-1} \text{ cm}^{-1}$, $\Phi_{\text{T}} = 0.20$)⁵⁶ being used as the reference.

Singlet Oxygen Quantum Yield Measurement. A PTI Quantamaster that is equipped with a Hamamatsu R5509-42 near-infrared (NIR) PMT was utilized to measure the singlet oxygen emission centered at 1268 nm from the 5 μM air-saturated (with an oxygen concentration of 21%) acetonitrile solutions of complexes Ir1–Ir6. The relative actinometry was used to determine the singlet oxygen quantum yields (Φ_{Δ}) of Ir1–Ir6 with [Ru(bpy)₃](PF₆)₂ in aerated CH₃CN ($\Phi_{\Delta} = 0.56$)⁵⁷ being used as the standard sample. The calculated Φ_{Δ} values were reproducible to within <5%.

Computational Methodology. The singlet ground-state geometries for all complexes were optimized using the density functional theory (DFT),⁵⁸ as implemented in the Gaussian16 software package.⁵⁹ The PBE1PBE functional⁶⁰ and the mixed basis set of LANL2DZ⁶¹ for Ir and 6-31G*⁶² for other elements were used for all ground-state calculations. It is a common practice to employ an effective core potential (ECP) basis such as LANL2DZ for transition metals because ECPs are parametrized to implicitly account for scalar relativistic (SR) effects, which are known to be significant for Ir. The solvent effect was incorporated using the conductor-like polarizable continuum model (CPCM),⁶³ with acetonitrile dielectric constant

being used as the solvent model to be consistent with the experimental conditions.

Linear response time-dependent DFT (TDDFT)⁶⁴ was utilized to calculate optical transitions. For these calculations, we modified the PBE1PBE functional by increasing the Hartree–Fock (HF) exchange part to 32%, which provided a better agreement with the experimental spectra of Ir1–Ir6. The mixed LANL2DZ/6-31G* basis set and CPCM/acetonitrile solvent model were used for excited-state calculations. The experimental UV–vis absorption spectra were simulated by calculating up to 70 optical transitions. The Gaussian function with a broadening parameter of 0.12 eV was used to obtain thermal broadening of each transition to match the line shapes of the experimental absorption spectra.

Emission energies were calculated by optimizing the lowest triplet excited state using the analytical gradient TDDFT. The same functional and basis sets used for calculations of the absorption spectra were employed for the emission energy calculations. Natural transition orbitals (NTOs)⁶⁵ were generated from the transition density matrices obtained from TDDFT calculations to demonstrate the nature of the electron–hole pairs contributing to each optical transition. All NTOs were visualized by VMD software⁶⁶ with a 0.02 isosurface. All calculations were carried out via a Gaussian16 software package.

Photobiological Activity Studies. The experimental details for cell culture, cytotoxicity/photocytotoxicity, confocal microscopy, and *in vitro* ROS generation on SK-MEL-28 cells and the *in vitro* cytotoxicity/photocytotoxicity on human breast cancer (MCF-7) cells and the *in vivo* antitumor evaluation on female Balb/c nude mice bearing the MCF-7 xenograft tumors are provided in the [Supporting Information](#).

It is worth noting that the PF₆[−] salts of the complexes were used for all of the photophysical studies and the singlet oxygen measurement, while the Cl[−] salts of the complexes were used for the photobiological activity studies for their better water solubility in aqueous solution.

RESULTS AND DISCUSSION

Electronic Absorption. Figure 1 displays the UV–vis absorption spectra (experimental and calculated ones) of complexes Ir1–Ir6 in acetonitrile solutions, and Table 1 lists the measured absorption band maxima and molar extinction coefficients. The corresponding experimental and calculated spectra were compared for each complex, and the results are provided in the [Supporting Information Figure S1](#).

The absorption followed the Beer's law in the concentration range (1×10^{-6} to 1×10^{-4} mol·L^{−1}) used in our study, indicating that no ground-state aggregation occurred in the tested concentration range. The spectra of all complexes share some common features: they all contain structured, high-energy absorption bands with large molar extinction coefficients at wavelengths <360 nm and a broad, featureless low-energy absorption band beyond this wavelength (for Ir1 the low-energy band does not separate as clearly from the high-energy absorption bands as those in the other complexes). Based on the spectral features and the molar extinction coefficients, we tentatively attribute the high-energy absorption bands to predominant ligand-localized ¹π,π* transitions and the low-energy broad band to predominant charge-transfer (¹CT) transitions. These assignments are partially supported by the solvent-dependent absorption spectral study on these complexes. As shown in Figure S2, the high-energy bands were not sensitive to the polarity of solvent, but the low-energy band was. The different responses of the high-energy and low-energy absorption bands to the solvent polarity change were in accordance with their respective ¹π,π* and ¹CT nature of these bands.

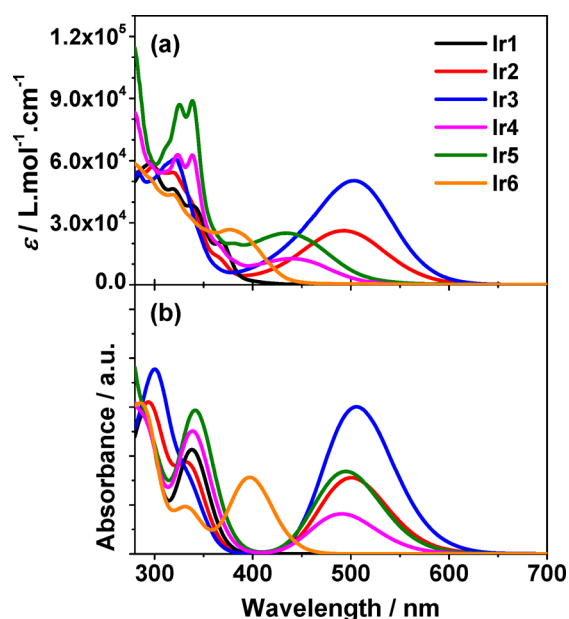


Figure 1. (a) Experimental and (b) calculated absorption spectra of Ir1–Ir6 in acetonitrile. Calculations were carried out by linear response TDDFT using the PBE1 hybrid functional with 32% HF coefficient and LANL2DZ/6-31G* basis sets. The simulated absorption spectra were obtained by Gaussian broadening of the calculated oscillation strength with a 0.12 eV line width.

It is apparent that the nature of the 4-Ar substituent(s) on the tpy ligand impacted the energy of the low-energy absorption band dramatically. Complexes Ir2 and Ir3 that contain the strong electron-donating 4'-N(CH₃)₂Ph substituent drastically red-shifted the low-energy absorption band compared to that in Ir1, and the molar extinction coefficient of this band in Ir3 is almost double that in Ir2. A similar phenomenon was observed in complexes Ir4 and Ir5 bearing the π -donating pyren-1-yl substituent. In complex Ir6, the relatively weaker electron-donating 4'-CH₃(OCH₂CH₂)₃OPh substituent also induced a well-separated charge-transfer absorption band at 375 nm compared to that of Ir1, but the shift to longer wavelength is not as drastic as those in complexes Ir2–Ir5. The electron-donating-substituent-induced charge-transfer absorption band was reported in other bis(terpyridine) Ir(III) complexes containing 4'-NH₂Ph or 4'-NMe₂Ph₂ substituents.^{41,42}

To unambiguously attribute the nature of the absorption bands, time-dependent density functional theory (TDDFT) calculations were conducted for complexes Ir1–Ir6 in CH₃CN. As Figure S1 in the [Supporting Information](#) indicated, the calculated absorption spectra matched the experimental results quite well with respect to both the energies and the spectral features. The obtained natural transition orbitals (NTOs) contributing to the major transitions of the low-energy absorption band and the high-energy absorption bands are given in Table 2 and [Supporting Information Table S2](#), respectively. As shown in Table 2, the lowest-energy transitions (S₁ state) for all complexes all possessed the intraligand charge transfer (¹ILCT)/metal-to-ligand charge transfer (¹MLCT)/¹π,π* configurations. However, the ¹ILCT contribution increased in the S₁ states of Ir2–Ir5 because of the increased electron-donating ability of the 4-Ar substituents in these complexes. In addition, ligand-to-ligand charge transfer (¹LLCT) also made a minor

Table 1. Electronic Absorption, Emission, and Triplet Excited-State Absorption Parameters for Complexes Ir1–Ir6

	$\lambda_{\text{abs}}/\text{nm}$ ($\log \epsilon$) ^a	$\lambda_{\text{em}}/\text{nm}$ ($\tau_{\text{em}}/\mu\text{s}$); Φ_{em} ^b	$\lambda_{\text{T}_1-\text{T}_n}/\text{nm}$ ($\tau_{\text{TA}}/\mu\text{s}$) ^c	Φ_{Δ} ($\lambda_{\text{ex}}/\text{nm}$) ^d
Ir1	296 (4.77); 318 (4.67); 338 (4.58); 369 (4.32)	494 (2.54), 519 (–); 0.32 ^e	389 (–), 636 (2.25)	0.14 (340)
Ir2	298 (4.76); 318 (4.73); 364 (4.11); 493 (4.42)	578 (3.13); <0.001	611 (0.009), 627 (3.12)	0.004 (475)
Ir3	283 (4.73); 310 (4.76); 320 (4.78); 503 (4.70)	– ^f	630 (0.008)	0.008 (478)
Ir4	280 (4.92); 323 (4.79); 338 (4.79); 440 (4.11)	577 (– ^g); 655 (– ^f); 0.008	444 (–), 528 (5.79)	0.81 (450)
Ir5	280 (5.06); 325 (4.94); 338 (4.95); 434 (4.40)	655 (– ^f); 0.004	444 (–), 527 (24.5)	0.75 (450)
Ir6	280 (4.77); 295 (4.71); 318 (4.64); 375 (4.42)	557 (7.92); 0.078	735 (8.15)	0.58 (386)

^a λ_{abs} refers to the electronic absorption band maxima, and ϵ indicates the molar extinction coefficients. The measurements were carried out in CH₃CN at room temperature. ^b λ_{em} and τ_{em} are the emission band maxima and lifetimes, respectively, at room temperature in degassed CH₃CN solutions ($c = 1 \times 10^{-5}$ mol·L⁻¹). For determining the emission quantum yields, the reference used was a degassed acetonitrile solution of [Ru(bpy)₃]Cl₂ ($\Phi_{\text{em}} = 0.097$, $\lambda_{\text{ex}} = 436$ nm) except for Ir1. ^cNanosecond TA band maxima ($\lambda_{\text{T}_1-\text{T}_n}$) and triplet excited-state lifetimes (τ_{TA}) measured in degassed CH₃CN at room temperature. ^dSinglet oxygen quantum yields in acetonitrile, with [Ru(bpy)₃](PF₆)₂ in aerated CH₃CN ($\Phi_{\Delta} = 0.56$) being used as the standard sample. The results are corrected to within $\pm 5\%$. ^eQuinine bisulfate ($\lambda_{\text{ex}} = 347.5$ nm, $\Phi_{\text{em}} = 0.546$) in 1 N H₂SO₄ solution was used as the reference. ^fEmission signals were too weak to be measured upon 355 nm excitation on our laser flash photolysis spectrometer, which is not optimized for emission measurements. ^gLifetime was too short to be measured on our instrument.

contribution to the low-energy absorption bands in these complexes. In contrast, the low-energy absorption band in Ir1 had more ¹ π, π^* character due to the weaker electron-donating ability of the Ph substituent compared to the substituents in Ir2–Ir6. For the high-energy absorption bands in the regions of 280–360 nm, the NTOs in Table S2 indicated predominant ligand-centered ¹ π, π^* transitions, admixing with some charge-transfer characters. Because of the strong intraligand charge-transfer nature of the low-energy absorption bands in Ir2–Ir6, the increased electron-donating ability of the 4-Ar substituent on tpy caused the significant red-shift of these absorption bands. The stronger the electron donor, the more red-shift of this band.

Photoluminescence. The emission characteristics of complexes Ir1–Ir6 were investigated at room temperature in a variety of solvents, including acetonitrile, tetrahydrofuran (with 1% acetonitrile), and dichloromethane (with 5% acetonitrile), and the normalized emission spectra in acetonitrile are displayed in Figure 2. A summary of the emission parameters, including the emission maxima (λ_{em}), lifetimes (τ_{em}), and quantum yields (Φ_{em}), is provided in Tables 1 and S3. The emission of Ir3 was too weak to be detected. Its emission spectrum and parameters are not included in Figure 2 and Tables 1 and S3.

All complexes except for Ir3 were emissive at room temperature in fluid solutions, and the emission wavelengths were much red-shifted (3024–8713 cm⁻¹) in comparison to their corresponding excitation wavelengths. Except for the short-wavelength shoulder at 577 nm in Ir4, the emission signals from Ir1, Ir2, and Ir6 decayed relatively slowly, with a lifetime of several microseconds, and the emission was prone to oxygen quenching. All these characteristics imply a phosphorescence nature of the emission from these complexes. In addition to this phosphorescence band, Ir4 possessed another emission band at 577 nm, which was not subject to oxygen quenching (Figure S4) and thus suggests fluorescence from the singlet excited state. The lifetime monitored at this wavelength was too short to be accurately determined on our instrument (<5 ns), in line with the fluorescence nature of this emission band. The appearance of both fluorescence and phosphorescence emission has been reported for a 4-(pyren-1-yl)tpy Pt(II) complex⁶⁷ and for a dinuclear Pt(II) terpyridine complex bridged with a fluorenyl group.⁶⁸

The emission spectrum of Ir1 displayed a well-resolved vibronic structure with a minor solvatochromic effect (Figure S5). With reference to the other Ir(III) terpyridine complexes

bearing alkylphenyl-substituted tpy ligand(s),^{40–42} the emitting state of Ir1 can be tentatively ascribed to the predominant ph-tpy-localized ³ π, π^* state. However, the shorter lifetime and the less salient vibronic structure of Ir1 in comparison to the emission from a pure ³ π, π^* emitting state suggest that the emitting state of Ir1 probably admixes some charge-transfer configurations, likely the ³MLCT/³ILCT configurations. In contrast to Ir1, the phosphorescence spectra of Ir2 and Ir6 were broad and lacked vibronic structures, and the solvatochromic effects were more obvious. Moreover, the emission quantum yields of these two complexes became much smaller. These characteristics imply the involvement of more charge-transfer characters in their emitting states. Considering the electron-donating nature of the dimethylamino and the oligoether groups on the ph-tpy frame in Ir2 and Ir6, ³ILCT could play a major role in the emitting triplet excited states. The involvement of the ³ILCT character caused the red-shifts of the emission bands and lowered the emission quantum yields because of the increased nonradiative decay rate that is intrinsically associated with the charge-transfer configuration. Note that Ir3 bearing two dimethylamino substituents on the ph-tpy ligands could have even more charge-transfer character in its emitting state, leading to an extremely weak luminescence that could not be detected. Due to the stronger electron-donating ability of the dimethylamino substituent than that of the oligoether group, stronger ³ILCT would be present in Ir2 compared to that in Ir6. Consequently, Ir2 exhibited a more red-shifted emission with a much lower quantum yield in comparison to those of Ir6.

Considering the phosphorescence in Ir4 and Ir5, although the spectra were featureless and much red-shifted and the emission signals were too weak to allow for the emission lifetimes to be determined (which all resembled the emission characteristics of Ir2 and Ir6), the emission energies were much less sensitive to the solvent polarity (which was similar to that of Ir1). Therefore, the emitting states in these two complexes might not involve much charge-transfer configuration. In view of the similar emission energy of these two complexes to those of other reported transition metal complexes containing pyrenyl-containing ligand,^{67,69–71} we tentatively attribute the observed phosphorescence from these two complexes to the pyrene-localized ³ π, π^* state.

The analytical TDDFT calculations on the lowest triplet excited states (T₁) of these complexes supported our aforementioned attributions to the nature of the emission. As shown in Table 3, the NTOs clearly revealed that the T₁ state

Table 2. Natural Transition Orbitals (NTOs) for the Major Transitions Contributing to the Low-Energy Absorption Band of Complexes Ir1–Ir6 in CH₃CN

	States	Hole	Electron
Ir1	S ₁ 338 nm <i>f</i> = 0.8886		
		55%	55%
		44%	44%
	S ₂ 337 nm <i>f</i> = 0.0060		
Ir2	S ₁ 500 nm <i>f</i> = 0.6113		
	S ₂ 497 nm <i>f</i> = 0.0508		
Ir3	S ₁ 505 nm <i>f</i> = 1.2774		
	S ₃ 479 nm <i>f</i> = 0.0001		
Ir4	S ₁ 490 nm <i>f</i> = 0.3467		
	S ₂ 448 nm <i>f</i> = 0.0028		
	S ₃ 447 nm <i>f</i> = 0.0005		
Ir5	S ₁ 495 nm <i>f</i> = 0.7150		
	S ₃ 448 nm <i>f</i> = 0.0038		
Ir6	S ₁ 397 nm <i>f</i> = 0.6640		
	S ₂ 381 nm <i>f</i> = 0.0006		

of Ir1 was dominated by the ³π,π* configuration, admixing with some ³MLCT/³ILCT/³LMCT configurations, whereas the T₁ states of Ir2 and Ir6 had increased ³ILCT contributions along with the ³π,π*/³MLCT/³LMCT configurations. In contrast, the holes of the T₁ states of Ir4 and Ir5 were exclusively on the pyrene motifs, while the electrons were delocalized to the central pyridine ring and very little to the d orbital of the Ir(III) ion in addition to the pyrene motifs. Therefore, the emitting T₁ states in Ir4 and Ir5 have almost exclusively pyrene-based ³π,π* character, admixing with very minor ³ILCT/³LMCT.

Transient Absorption (TA). To further understand the triplet excited-state characteristics of complexes Ir1–Ir6, especially for those complexes that do not emit or are weakly emissive, the nanosecond TA of these complexes was investigated in nitrogen-purged acetonitrile solutions. Figure

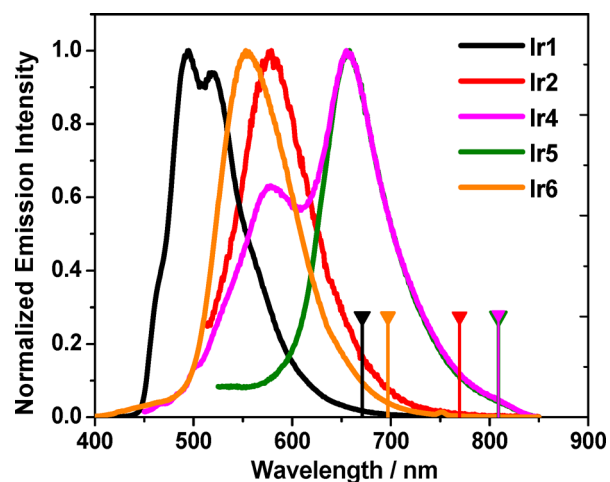


Figure 2. Emission spectra of Ir1 ($\lambda_{\text{ex}} = 369$ nm), Ir2 ($\lambda_{\text{ex}} = 492$ nm), Ir4 ($\lambda_{\text{ex}} = 434$ nm), Ir5 ($\lambda_{\text{ex}} = 434$ nm), and Ir6 ($\lambda_{\text{ex}} = 375$ nm) measured at room temperature in nitrogen-purged acetonitrile ($c = 1 \times 10^{-5}$ mol·L⁻¹) and calculated optimized T₁ energy (triangle headed bar). The emission of Ir3 was too weak to be detected. All energies were calculated by the optimized excited triplet state by using PBE1 with 32% HF exchange coefficient, LANL2DZ/6-31G* basis sets, and acetonitrile solvent. Bar heights and thickness are arbitrary.

Table 3. NTOs of the Lowest Triplet Excited State (T₁) of Ir1–Ir6 in CH₃CN^a

	T ₁ / nm	Hole	Electron
Ir1	671		
Ir2	769		
Ir4	780		
Ir5	782		
Ir6	697		

^aModified PBE1 functional with 32% HF exchange coefficient and LANL2DZ/6-31G* basis sets were used for the calculations.

3 shows the TA spectra of Ir1–Ir6 at zero delay after 355 nm excitation. The time-resolved spectra for each complex are provided in Figure S6 of the Supporting Information. The TA parameters, such as the TA band maxima and the triplet excited-state lifetimes by monitoring the decay of TA signals, are summarized in Table 1.

The deduced TA lifetimes of Ir1 and Ir6 are similar to their emission lifetimes in acetonitrile, implying that the transient absorbing excited states in these two complexes are the emitting states. Probably due to the increased ³ILCT contribution to the T₁ state of Ir6, its TA band maximum was much red-shifted compared to that of Ir1, accompanied by the appearance of clear bleaching at the wavelength that was in accordance with its ¹ILCT/¹π,π* absorption band. For Ir2, its

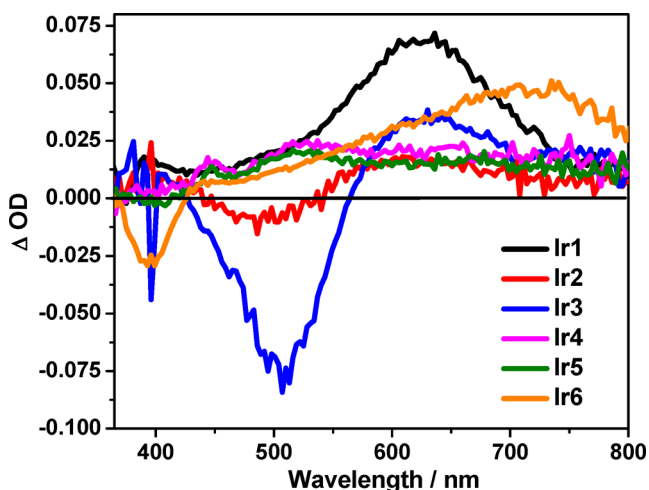


Figure 3. Nanosecond transient differential absorption spectra of Ir1–Ir6 in nitrogen-purged acetonitrile at zero delay after 355 nm excitation. $A_{355} = 0.4$ in a 1 cm cuvette.

TA signal consisted of two components with distinct decay kinetics (Figure S6): the fast-decayed signal had a lifetime of 9 ns, and the slow one had a lifetime of 3.12 μ s, which was consistent with its emission lifetime. For Ir3, its TA signals were stronger than those in Ir2 but decayed with a lifetime (8 ns) similar to that of the fast component in Ir2. The fast decaying TA spectrum of Ir2 was quite similar to that of Ir3, with the similar TA band maxima and the similar bleaching occurring at their corresponding $^1\text{ILCT}/^1\pi,\pi^*$ absorption bands. Thus, we presumably assign these TAs to predominant $^3\text{ILCT}$ states. In contrast, the slower decayed TA spectral feature of Ir2 resembled that of Ir1. In view of the similar lifetime of this long-lived TA species to its emission lifetime, we ascribe the slower TA component emanating from the

$^3\text{ILCT}/^3\pi,\pi^*/^3\text{MLCT}/^3\text{LMCT}$ T_1 state of Ir2. The observation of the rapid conversion of the short-lived transient species to the long-lived species in Ir2 implies that the high-lying $^3\text{ILCT}$ state was populated first, and then it decayed to the long-lived T_1 state. The TA spectra of Ir4 and Ir5 resembled each other with long lifetimes, suggesting the similar origin of the transient absorbing states. Considering the same nature of the T_1 states in these two complexes and the similar TA spectral feature to that reported for a Pt(II) complex bearing a pyrenyl-acetylide ligand,⁷¹ we attribute the observed TA to the pyrenyl-localized $^3\pi,\pi^*$ states. It is noted that the TA lifetime of Ir5 is almost 1 order of magnitude longer than that of Ir4, although their T_1 states are both localized on the pyrenyl component. A careful examination of the NTOs in Table 3 for the T_1 states of Ir4 and Ir5 revealed that Ir4 contains slightly more $^3\text{ILCT}$ character in its T_1 state. The slightly more charge-transfer character in the T_1 state of Ir4 may reduce its T_1 lifetime. Alternatively, the dual emission of Ir4 implies that the fluorescent ^1CT state lies in proximity of the T_1 state, which hypothetically allows for the coupling between these two states but does not reach an equilibrium. Consequently, the T_1 lifetime of Ir4 was reduced.

Singlet Oxygen Generation. Singlet oxygen generation is an important property for photobiological applications such as PDT that rely on cytotoxic ROS. Therefore, the singlet oxygen quantum yields (Φ_Δ) were evaluated for Ir1–Ir6. These measurements were carried out in CH_3CN relative to $[\text{Ru}(\text{bpy})_3](\text{PF}_6)_2$ as the standard ($\Phi_\Delta = 56\%$)⁵⁷ using the inherent luminescence of $^1\text{O}_2$ centered at approximately 1270 nm. The reason that Φ_Δ was measured in CH_3CN as the solvent (rather than water or aqueous solutions) is because water quenches the emission from $^1\text{O}_2$, precluding the accurate determination of Φ_Δ .⁷² In addition, pure water is not representative of a real biological environment, where it is expected that the complexes would be associated with

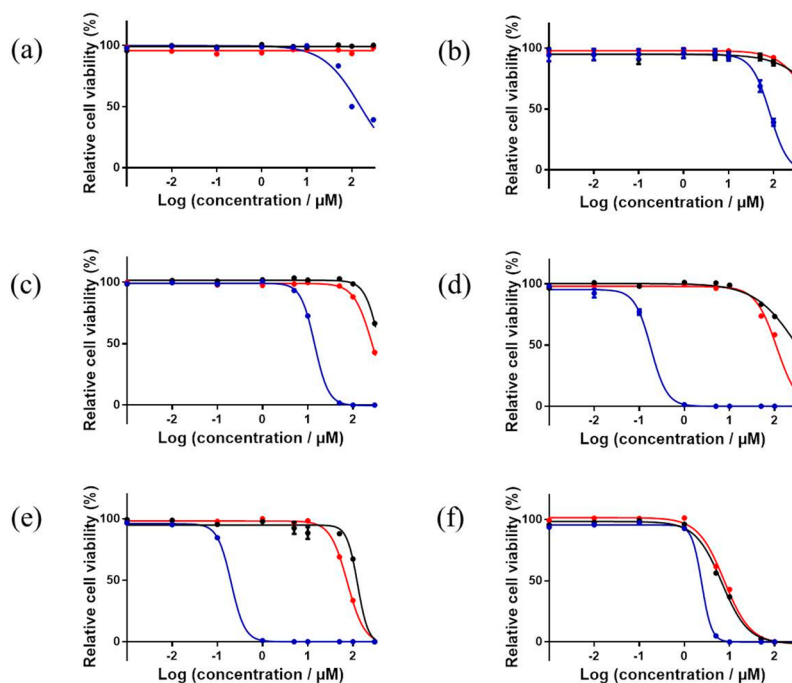


Figure 4. *In vitro* dose–response curves for complexes Ir1 (a), Ir2 (b), Ir3 (c), Ir4 (d), Ir5 (e), and Ir6 (f) in SK-MEL-28 cells without (black) or with visible (blue) or red (red) light irradiation.

biological macromolecules and thus experience greater hydrophobicity as a result. Although Φ_{Δ} in the real biological environment cannot be known with certainty, the measurement in CH_3CN allows us to assess the potential of the complexes for producing $^1\text{O}_2$ and compare this ability with other complexes in the literature, which are routinely reported in CH_3CN .

Excitation spectra were collected for **Ir1–Ir6** with $\lambda_{\text{em}} = 1268$ nm, and the excitation maxima were used as the excitation wavelengths in the emission measurement. The values for Φ_{Δ} using the corresponding excitation maximum for each complex are listed in Table 1. In this way, Φ_{Δ} represents the maximum efficiency for $^1\text{O}_2$ generation in CH_3CN provided the most effective excitation wavelength is used. In actual photobiological assays, however, broadband visible light was used. Generally speaking, the excitation maxima for $^1\text{O}_2$ emission positively correlated with the longest wavelength maximum in the absorption spectra, with **Ir2** and **Ir3** generating more $^1\text{O}_2$ with longer excitation wavelengths (>450 nm), **Ir1** and **Ir6** requiring shorter wavelengths (<400 nm), and the **Ir4** and **Ir5** intermediate at approximately 450 nm.

Within this small family of complexes, changes in the 4-R-tpy groups had marked effects on $^1\text{O}_2$ yields and proved to be a facile way to tune this parameter and better understand the nature of the excited states involved. The $^1\text{O}_2$ quantum yields were largest for the pyrenyl-containing complexes **Ir4** and **Ir5**, with one pyrenyl group in **Ir4** being slightly more effective than two in **Ir5** (81% versus 75%). The dimethylaminophenyl substituents had detrimental effects on Φ_{Δ} , whereby **Ir2** and **Ir3** were less than 1%, and even $\text{R}_1=\text{R}_2=\text{Ph}$ (**Ir1**) showed marked attenuation ($\Phi_{\Delta} = 14\%$). Interestingly, when one Ph group in **Ir1** was replaced with the water-solubilizing polyether substituent in **Ir6**, the $^1\text{O}_2$ quantum yield increased 4-fold. The pyrenyl group is known to have an effective triplet state of π,π^* character for generating $^1\text{O}_2$, so the large values for Φ_{Δ} with **Ir4** and **Ir5** were in line with expectations and justified the use of these groups as substituents despite their hydrophobicities. The relatively large $^1\text{O}_2$ quantum yields for **Ir4** and **Ir5** positioned these complexes as potentially good photobiological agents.

Cytotoxicity and Photocytotoxicity toward Human Melanoma (SK-MEL-28) Cancer Cells. The six complexes of this family were explored for their cytotoxicities and photobiological activities using the SK-MEL-28 human skin melanoma cancer cell line (Figure 4). Briefly, cells were dosed with the complex in the range of 1 nM to 300 μM and incubated at 37 °C (5% CO_2) for approximately 16 h before receiving a dark or light treatment. Excess PS was not removed before delivering the light treatment in order to capture any photoactivated uptake that may occur.

The light treatments were either broadband visible light of 100 J cm^{-2} or monochromatic red light (625 nm) of the same fluence. The cells were incubated again following the dark or light treatment and quantified with the resazurin cell viability dye at 48 h.⁷³ Cytotoxicity and photocytotoxicities are reported in Table 4 as the effective concentration of complex to reduce cell viability to 50%, EC_{50} , in this assay, and the phototherapeutic indices (PIs) are the ratios of the dark to light EC_{50} values and represent the amplification of cytotoxicity with the light treatment.

Ir1–Ir4 were nontoxic to cells over the concentration range tested, and thus EC_{50} values were estimated as >300 μM , with

Table 4. EC_{50} Values (μM) for SK-MEL-28 Cancer Cells Dosed with Complexes **Ir1–Ir6**

	dark	vis ^a	PI ^b	red ^c	PI ^d
Ir1	>300	153 ± 15	>2	>300	1
Ir2	>300	83.4 ± 4.2	>4	>300	1
Ir3	>300	14.2 ± 0.2	>21	266	>1
Ir4	>300	0.18 ± 0.01	>1657	112 ± 4	>3
Ir5	127 ± 5	0.20 ± 0.01	628	75.1 ± 1.1	2
Ir6	6.72 ± 0.22	2.42 ± 0.08	3	7.65 ± 0.29	1

^aVis-PDT: 16 h drug-to-light interval followed by 100 J cm^{-2} broadband visible-light irradiation. ^bPI = phototherapeutic index (ratio of dark EC_{50} to visible-light EC_{50}), ^cRed-PDT: 16 h drug-to-light interval followed by 100 J cm^{-2} light irradiation with 625 nm LEDs. ^dPI = phototherapeutic index (ratio of dark EC_{50} to red-light EC_{50}).

precise determination limited by the insolubilities of the complexes in the assay media at higher concentrations. **Ir5** was slightly more toxic than **Ir1–Ir4** but relatively nontoxic overall with an EC_{50} greater than 100 μM . Interestingly, **Ir6** was cytotoxic without a light treatment ($\text{EC}_{50} = \sim 7$ μM), underscoring that the polyethoxy substituent that was incorporated to enhance aqueous solubility resulted in high baseline cytotoxicity and would limit the utility of the complex as a photobiological agent despite an $^1\text{O}_2$ quantum yield of almost 60%. The origin of this cytotoxicity was not investigated further as part of the present study.

All of the complexes exhibited enhanced cytotoxicity with visible light, albeit to significantly different degrees. The 2- to 4-fold enhancement for **Ir1–Ir2** and **Ir6** was not large enough to qualify these complexes for further study as photobiological agents. Likewise, the modest PI of >21 and the low photocytotoxicity ($\text{EC}_{50} = \sim 14$ μM) of **Ir3** were not notable. However, the pyrenyl-containing complexes **Ir4** and **Ir5** had submicromolar EC_{50} values that were similar (180 and 200 nM, respectively) and large PIs. **Ir4** that was nontoxic in the dark had the largest PI of the series at >1657, which positively correlated with its $^1\text{O}_2$ quantum yield (Figure 5). The slightly higher dark cytotoxicity of **Ir5** led to a reduced PI of 628, but this number is still considered quite large relative to most PDT agents.

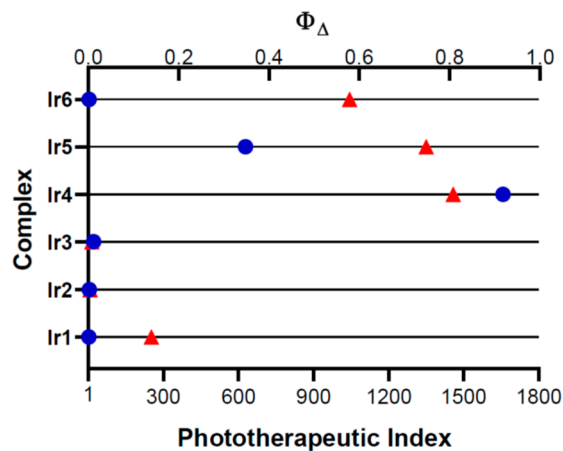


Figure 5. Correlation chart between the cell-free $^1\text{O}_2$ quantum yields (red triangles) and the *in vitro* PIs (blue circles) for complexes **Ir1–Ir6**.

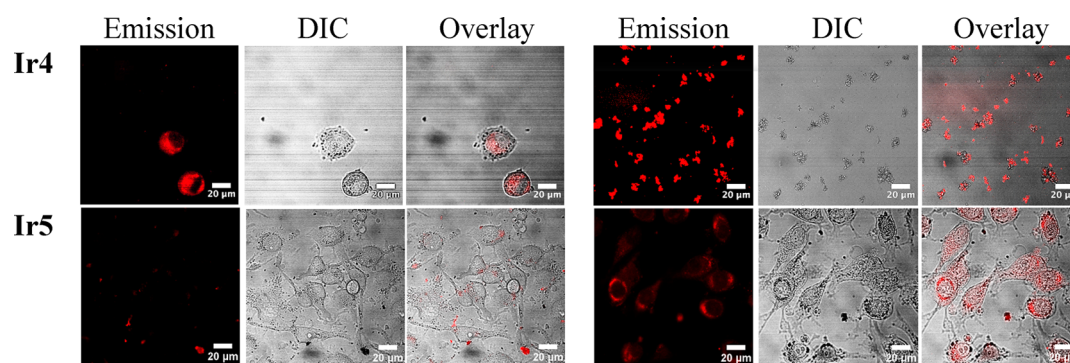


Figure 6. Confocal luminescence images of SK-MEL-28 cells dosed with complexes Ir4 and Ir5 ($50 \mu\text{M}$) in the dark (left) and with visible light (50 J cm^{-2}) (right).

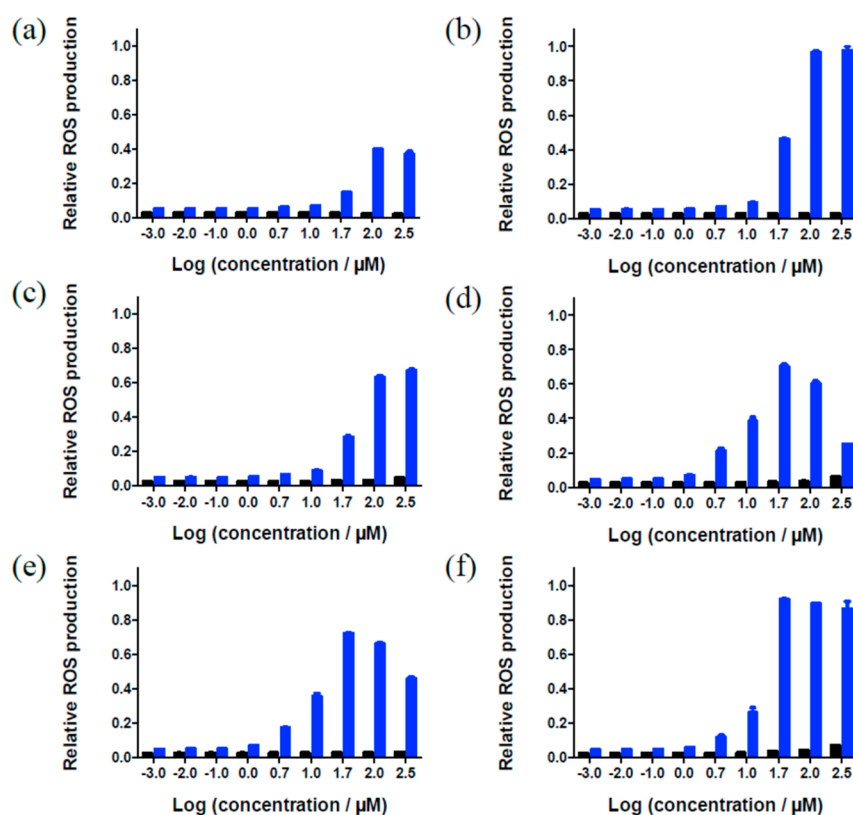


Figure 7. ROS assay results (60 min post-treatment) for SK-MEL-28 cells treated with Ir1 (a), Ir2 (b), Ir3 (c), Ir4 (d), Ir5 (e), and Ir6 (f). DCFDA was used as an ROS probe. The black bars and blue bars represent the results for cells treated in the dark or with 50 J cm^{-1} visible light, respectively.

While Ir4 and Ir5 had very slight enhancements of their cytotoxicities with 625 nm light (PIs on the order of 2–3), none of the complexes could be considered as PDT agents with red light. Therefore, the very high potencies with visible light are presumably due to the shorter wavelengths in the visible spectrum, and thus these complexes would be best suited for applications requiring superficial activation of PSs with blue or green light. The potent *in vitro* photobiological effects of Ir4 and Ir5, the pyrenyl-based complexes of the series, further illustrate the utility of highly photosensitizing $^3\pi,\pi^*$ states that have been previously documented for PDT.⁵

Cells treated with Ir4 and Ir5 at $50 \mu\text{M}$ were observed by laser scanning confocal microscopy after a dark or a visible-light treatment of 50 J cm^{-2} (Figure 6). The light condition was chosen such that enough cells remained for viewing. The

inherent luminescence from Ir4 was visible in the cytosol of the dark-treated cells, and the dead/dying cells and cellular debris remaining after light treatment were highly luminescent. Even in the dark, cells treated with Ir4 underwent morphological changes from elongated and spindle-shaped to detached and spherical. Under the same treatment conditions, Ir5 appeared to be taken up by cells in the dark less readily based on luminescence as an indicator. The cells dosed with Ir5 and treated with visible light, however, displayed bright luminescence from the cytosol with accumulation possibly in the mitochondria. Treatment of cells with Ir5 under both dark and light conditions resulted in a few morphological changes at the observation time point. It is interesting to note that the cells appeared healthier upon treatment with Ir5 despite the

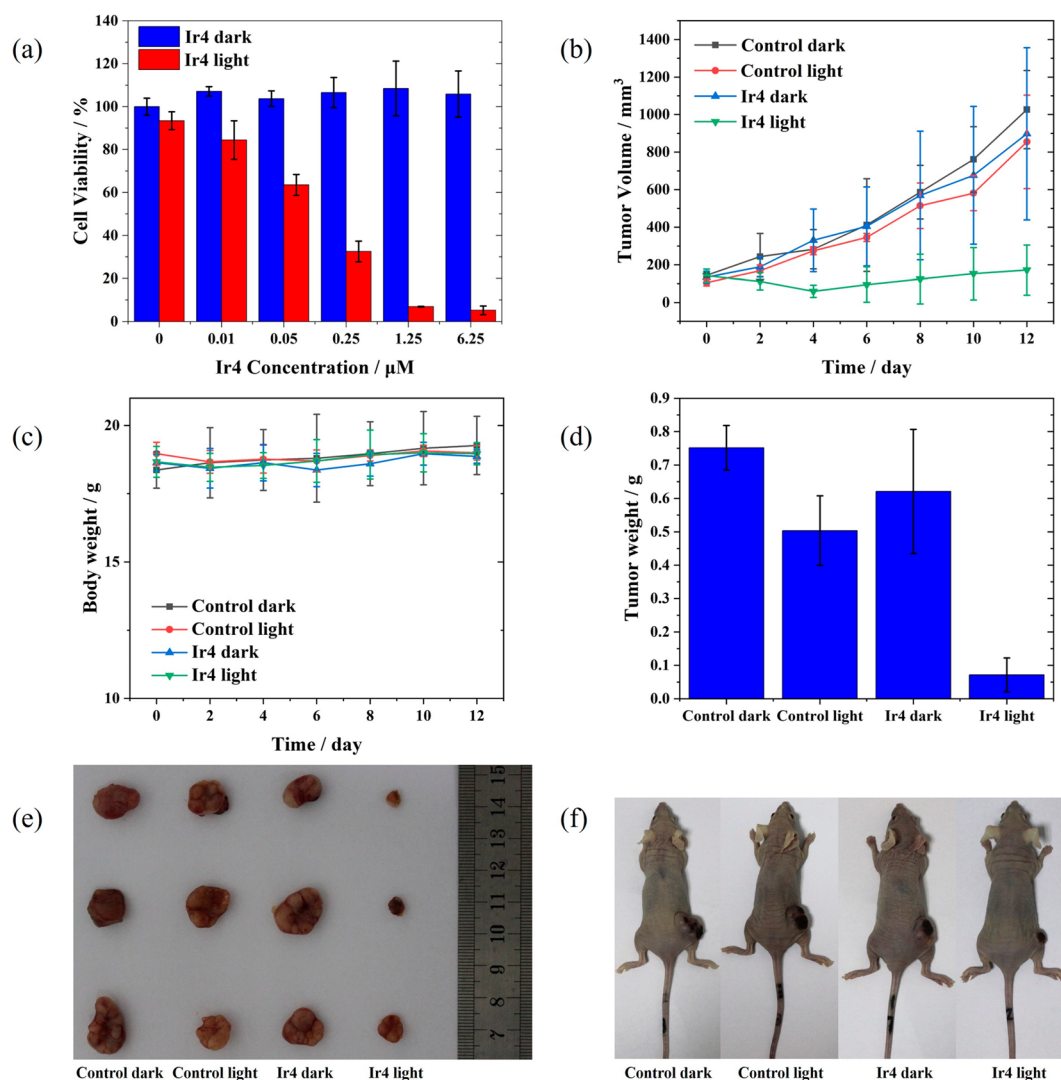


Figure 8. (a) Dose-dependent cell viability study of Ir4 toward MCF-7 breast cancer cells. The light treatment used a 450 nm, 50 mW cm^{-2} blue light to irradiate for 5 min (15 J cm^{-2}). (b) Tumor growth curves of the four differently treated mouse groups. (c) Body weight changes of the four differently treated mouse groups. (d) Comparison of the tumor weight 12 days after different treatments. (e) Photographs of tumors collected from the mice 12 days after the different treatments. (f) Photographs of tumor-bearing mice 12 days after the different treatments. In panels b–f, all of the light treatments used a 450 nm, 100 mW cm^{-2} blue light to irradiate for 10 min (60 J cm^{-2}).

higher dark toxicity measured in the dose–response assay for this complex.

The confocal experiments cannot definitively establish cellular localization since the experiment relies on luminescence from the complex, which in turn is dependent on environment, but they do highlight the potential of the complexes to act as theranostic agents despite emission quantum yields of $<1\%$ in cell-free conditions. The number of pyrenyl units incorporated into the $\text{Ir}(\text{R-tpy})_2^{3+}$ scaffold appears to influence uptake, localization, and cellular responses and, consequently, cytotoxicity and photocytotoxicity. However, the observations in the confocal experiments did not have a clear correlation with the dose–response outcomes given that Ir5 was slightly more cytotoxic with a smaller PI in the dose–response assays.

In Vitro ROS Detection in Treated Human Melanoma (SK-MEL-28) Cancer Cells. The photobiological activities associated with the complexes, notably Ir4 and Ir5, were attributed to ROS generation, specifically $^1\text{O}_2$. As expected, the photocytotoxicities toward SK-MEL-28 cells correlated well

with values measured for Φ_Δ under cell-free conditions. However, other ROS could also be involved (e.g., superoxide anion, hydrogen peroxide, hydroxyl radical), so the highly sensitive 2',7'-dichlorodihydrofluorescein diacetate (DCFDA) fluorophore⁷⁴ was used as a general probe for reporting on ROS production in live cells (Figure 7). This assay is based on the cell-permeable DCFDA being deacetylated by cellular esterases to its nonfluorescent analogue, which reacts with ROS to yield the oxidized DCF product that is highly fluorescent.

To probe for ROS production by Ir1–Ir6 in the dark and with visible-light activation, SK-MEL-28 cells were preincubated with DCFDA and then subjected to the assay described for (photo)cytotoxicity except that a sublethal light treatment was used to ensure a proportion of live cells for intracellular ROS quantification. Fluorescence from DCF was markedly enhanced with visible-light treatment for all of the complexes. The complex that produced the maximum fluorescence from DCF was Ir2, which had the smallest $^1\text{O}_2$ quantum yield of the series and one of the largest EC_{50} values (corresponding to

lowest photobiological activity). However, these maximal values occurred at a very high concentration of PS ($>300 \mu\text{M}$). It is more informative to compare the onset of ROS production among the complexes, whereby **Ir4** and **Ir5** produce the onset of DCF fluorescence at the lowest concentrations. For example, at $5 \mu\text{M}$ and $10 \mu\text{M}$, **Ir4** and **Ir5** clearly induced more DCF fluorescence than the other complexes. The onset of DCF fluorescence is important because once cells begin to die the DCF fluorescence decreases. Consequently, the concentration at which maximal DCF fluorescence is observed for a compound (rather than the maximum value itself) is also informative. The earlier this occurs, the more potent the PS in terms of ROS production. For **Ir4** and **Ir5**, it occurs at $50 \mu\text{M}$ with decreases thereafter. **Ir6** is the only other complex in the series that has a similar onset (maximal at $50 \mu\text{M}$) of DCF fluorescence. However, its dark cytotoxicity negates any enhanced toxicity that might be gained through photosensitized ROS production.

The intracellular ROS assay also points toward **Ir4** and **Ir5** as being the most potent PSs of the series, underscoring the importance of the pyrenyl units to the photobiological activities of this class of complexes. The agreement between the cell-free $^1\text{O}_2$ quantum yields and the onset of detectable *in vitro* ROS production points toward cytotoxic $^1\text{O}_2$ as perhaps the most important ROS mediator and suggests PDT as the underlying mechanism.

In Vitro and In Vivo PDT Studies Using Human Breast (MCF-7) Cancer Cells and Tumor Xenografts. The promising *in vitro* photobiological activity of **Ir4** toward SK-MEL-28 cells, specifically the strong PDT effect, warranted further investigation. To probe the robustness of the response, we tested its effectiveness toward a different cell line with a different light source and protocol. Further, we tested this response in the more clinically relevant mouse xenograft model. Blue light (450 nm , 50 or 100 mW cm^{-2}) was used because the lowest-energy absorption band of **Ir4** occurred at 440 nm , and thus that is where the maximum response might be expected. We wish to show proof-of-concept and recognize that clinical applications would mostly likely require longer wavelengths and possibly optimized structures.

The PDT effects of **Ir4** toward the MCF-7 breast cancer cell line and on the corresponding MCF-7 xenografts implanted on the Balb/c nude mice ($16\text{--}18 \text{ g}$) were investigated. **Figure 8a** shows the cell viability comparison with and without light treatment upon incubation with increasing doses of **Ir4**. There was no dark toxicity over the tested concentration range; however, cells treated with **Ir4** and irradiated with 450 nm light (50 mW cm^{-2}) for 5 min (15 J cm^{-2}) were destroyed in a dose-dependent manner. Notably, the cell viability decreased to approximately 5% with only 5 min of irradiation at low micromolar concentrations of **Ir4**. The EC_{50} value against MCF-7 cells using this light condition was as low as $0.092 \mu\text{M}$.

We next tested whether **Ir4** and blue light could be effective for treating solid tumors with PDT in a mouse model. MCF-7 cells were implanted in the right flank of female Balb/c nude mice ($16\text{--}18 \text{ g}$) to establish the xenograft solid tumors. When the tumor size reached $100\text{--}150 \text{ mm}^3$, the mice were randomly divided into four groups with three mice in each group before the experiment: i.e., the control group without any treatment (control dark), the control group only with blue light irradiation (control light), the treatment group only with **Ir4** injection (**Ir4** dark), and the PDT treatment group with **Ir4** injection and blue light activation (**Ir4** light). **Ir4** was

injected directly into the tumor (10 mg kg^{-1} , $100 \mu\text{L}$) in PET (6% polyethylene glycol 400, 3% ethanol, 1% Tween 80 and 90% PBS) for the two treatment groups. For the PDT treatment, one hour after the injection, the blue light (450 nm , 100 mW cm^{-2}) was delivered to the tumor site for 10 min (60 J cm^{-2}).

The tumor volume and weight of the mice were monitored every 2 days, and the data for the 12 day post treatment period are provided in **Figures 8b** and **8c**. The tumor weight comparison to the control groups at 12 days post treatment is provided in **Figure 8d**, and the separated solid tumors and the whole body images are shown in **Figures 8e** and **8f**. **Figures 8b–f** demonstrate a measurable *in vivo* PDT effect on the MCF-7 xenograft tumors.

Tumor growth was dramatically inhibited, with essentially no change in tumor volume 12 days after the PDT treatment and tumor weight limited to approximately 10% compared to the control group that did not receive **Ir4** or a light treatment. The PDT treatment had almost no impact on the body weight gain of the mice, reflected by the similar body weight of the PDT treatment group with respect to the three control groups (**Figure 8c**). In fact, the slight increase in body weight for the control and treatment groups highlights the low dark toxicity of **Ir4**, the good tolerance of PDT, and the negligible side effects of the treatment.

CONCLUSIONS

We presented the synthesis, photophysics, and photobiological studies of a series of tricationic mononuclear homoleptic or heteroleptic bis(terpyridine) Ir(III) complexes with various substituents at the 4-position of tpy. Compared to the parent complex (**Ir1**), the low-energy absorption bands for the rest of the complexes were gradually red-shifted, which are directly controlled by the different electron-donating abilities of the substituents. The stronger donors also stabilized the triplet emitting states and resulted in much weaker phosphorescence owing to the accelerated nonradiative decay rate. All complexes, except for **Ir3**, exhibited broad positive absorption bands in the visible and extending to the NIR region. The long-lived transient species in complexes **Ir4** and **Ir5** had a lifetime of ca. 5.8 and $24 \mu\text{s}$, respectively, which makes them suitable candidates for PDT study.

In fact, the complexes with the longest TA lifetimes (**Ir4** and **Ir5**) were also the strongest $^1\text{O}_2$ generators under cell-free conditions, exhibited the most potent photobiological activities toward SK-MEL-28 cells, and appeared to be the most effective ROS producers *in vitro*. The pyrenyl group is clearly an important substituent for eliciting potent *in vitro* PDT effects, presumably due to the increased π, π^* character of the lowest-lying triplet excited states, which is known to prolong excited-state lifetimes. Notably, the lifetime of the $^3\pi, \pi^*$ state in **Ir4** is about ten times shorter than that for **Ir5**, possibly due to increased $^3\text{ILCT}$ character and/or coupling to ^1CT states of similar energy. Nevertheless, **Ir4** had the largest PI and was more than 2-fold greater than that for **Ir5** due to its reduced dark cytotoxicity. The PI of >1657 is the strongest antiproliferative activity so far among the reported visible-light-stimulated Ir(III) complexes. **Ir4** also exhibited a very strong *in vitro* PDT effect toward MCF-7 breast cancer cells and dramatically inhibited the xenograft tumor growth upon 450 nm light activation with essentially no dark toxicity and negligible side effects upon PDT treatment. Importantly, activity with **Ir4** was demonstrated using different light sources

between two laboratories across two different cell lines as well as a tumor xenograft model, further validating our findings. These results demonstrate the potential of Ir4, and possible other Ir(III) bis(terpyridine) complexes, as PDT agents.

■ ASSOCIATED CONTENT

🔗 Supporting Information

The Supporting Information is available free of charge on the ACS Publications website at DOI: 10.1021/acsabm.9b00312.

Experimental details for the PDT studies on SK-MEL-28 cells and on MCF-7 breast cancer cells and its xenograft tumor model; comparison of the UV–vis absorption spectra obtained experimentally and by calculation for complexes Ir1–Ir6 in CH₃CN; the normalized UV–vis absorption and emission spectra of Ir1–Ir6 in different solvents; the comparison of the emission spectra of Ir4 in aerated and deaerated acetonitrile solutions; the natural transition orbitals (NTOs) for the major transitions contributing to the absorption bands of Ir1–Ir6 at 280–360 nm in CH₃CN; the emission characteristics of Ir1–Ir6 in different solvents; and the time-resolved nanosecond transient absorption spectra of Ir1–Ir6 in CH₃CN (PDF)

■ AUTHOR INFORMATION

Corresponding Authors

*E-mail: wenfang.sun@ndsu.edu. Tel.: 701-231-6254. Fax: 701-231-8831.

*E-mail: samcfarl@uncg.edu. Tel.: 336-256-1080. Fax: 336-334-5402.

*E-mail: jian.tian@whu.edu.cn.

ORCID

Bingqing Liu: 0000-0002-1540-2235

Mohammed A. Javed: 0000-0001-8552-0301

Colin G. Cameron: 0000-0003-0978-0894

Svetlana Kilina: 0000-0003-1350-2790

Sherri A. McFarland: 0000-0002-8028-5055

Wenfang Sun: 0000-0003-3608-611X

Notes

The authors declare no competing financial interest.

■ ACKNOWLEDGMENTS

W. Sun and S. Kilina acknowledge the financial support from the National Science Foundation (DMR-1411086 and CHE-1800476) for complex synthesis, characterization, and computational simulation of the optical spectra. S. Kilina is grateful to the US Department of Energy (DE-SC008446) for partial financial support of the method development and Center for Computationally Assisted Science and Technology (CCAST) at the North Dakota State University and the National Energy Research Scientific Computing Center (NERSC) allocation Award No. 86678 (supported by the Office of Science of the Department of Energy under Contract No. DE-AC02-05CH11231) for computer access and administrative support. The photobiological studies on the SK-MEL-28 cells reported in this publication were supported by the National Cancer Institute of the National Institutes of Health under Award Number R01CA222227 to S. A. McFarland. The content is solely the responsibility of the authors and does not necessarily represent the official views of the National Institutes of Health. S. A. McFarland also acknowledges

financial support from the University of North Carolina at Greensboro, the Natural Sciences and Engineering Council of Canada, and Acadia University. J. Tian thanks the National Natural Science Foundation of China (Grants 21601140 and 21871214) for supporting his part of the work on the breast cancer cells and xenograft tumor model. We also thank Wan Xu in Sun's group at NDSU for her help in checking some of the photophysical data that are not included in this paper.

■ REFERENCES

- (1) Celli, J. P.; Spring, B. Q.; Rizvi, I.; Evans, C. L.; Samkoe, K. S.; Verma, S.; Pogue, B. W.; Hasan, T. Imaging and Photodynamic Therapy: Mechanisms, Monitoring, and Optimization. *Chem. Rev.* **2010**, *110*, 2795–2838.
- (2) Shi, G.; Monro, S.; Hennigar, R.; Colpitts, J.; Fong, J.; Kasimova, K.; Yin, H.; DeCoste, R.; Spencer, C.; Chamberlain, L.; Mandel, A.; Lilge, L.; McFarland, S. A. Ru(II) Dyads Derived from α -Oligothiophenes: A New Class of Potent and Versatile Photosensitizers for PDT. *Coord. Chem. Rev.* **2015**, *282–283*, 127–138.
- (3) Li, X.; Lee, S.; Yoon, J. Supramolecular Photosensitizers Rejuvenate Photodynamic Therapy. *Chem. Soc. Rev.* **2018**, *47*, 1174–1188.
- (4) Wilson, B. C.; Patterson, M. S. The Physics, Biophysics and Technology of Photodynamic Therapy. *Phys. Med. Biol.* **2008**, *53*, R61–R109.
- (5) Monro, S.; Colón, K. L.; Yin, H.; Roque, J.; Konda, P.; Gujar, S.; Thummel, R. P.; Lilge, L.; Cameron, C. G.; McFarland, S. A. Transition Metal Complexes and Photodynamic Therapy from a Tumor-Centered Approach: Challenges, Opportunities, and Highlights from the Development of TLD1433. *Chem. Rev.* **2019**, *119*, 797–828.
- (6) Bellnier, D. a; Dougherty, T. J. A Preliminary Pharmacokinetic Study of Intravenous Photofrin in Patients. *J. Clin. Laser Med. Surg.* **1996**, *14*, 311–314.
- (7) Allison, R. R.; Sibata, C. H. Oncologic Photodynamic Therapy Photosensitizers: A Clinical Review. *Photodiagn. Photodyn. Ther.* **2010**, *7*, 61–75.
- (8) Dolmans, D. E. J. G. J.; Fukumura, D.; Jain, R. K. Photodynamic Therapy for Cancer. *Nat. Rev. Cancer* **2003**, *3*, 380–387.
- (9) Gomer, C. J.; Razum, N. J. Acute Skin Response in Albino Mice Following Porphyrin Photosensitization Under Oxidic and Anoxic Conditions. *Photochem. Photobiol.* **1984**, *40*, 435–439.
- (10) Abrahamse, H.; Hamblin, M. R. New Photosensitizers for Photodynamic Therapy. *Biochem. J.* **2016**, *473*, 347–364.
- (11) Zhang, J.; Jiang, C.; FigueiróLongo, J. P.; Azevedo, R. B.; Zhang, H.; Muehlmann, L. A. An Updated Overview on the Development of New Photosensitizers for Anticancer Photodynamic Therapy. *Acta Pharm. Sin. B* **2018**, *8*, 137–146.
- (12) Sternberg, E. D.; Dolphin, D. Second Generation Photodynamic Agents: A Review. *J. Clin. Laser Med. Surg.* **1993**, *11*, 233–241.
- (13) Kataoka, H.; Nishie, H.; Hayashi, N.; Tanaka, M.; Nomoto, A.; Yano, S.; Joh, T. New Photodynamic Therapy with Next-Generation Photosensitizers. *Ann. Transl. Med.* **2017**, *5*, 183.
- (14) Ormond, A. B.; Freeman, H. S. Dye Sensitizers for Photodynamic Therapy. *Materials* **2013**, *6*, 817–840.
- (15) Bagchi, D.; Bhattacharya, A.; Dutta, T.; Nag, S.; Wulferding, D.; Lemmens, P.; Pal, S. K. Nano MOF Entrapping Hydrophobic Photosensitizer for Dual-Stimuli-Responsive Unprecedented Therapeutic Action against Drug-Resistant Bacteria. *ACS Appl. Bio Mater.* **2019**, *2*, 1772–1780.
- (16) Mari, C.; Pierroz, V.; Ferrari, S.; Gasser, G. Combination of Ru(II) Complexes and Light: New Frontiers in Cancer Therapy. *Chem. Sci.* **2015**, *6*, 2660–2686.
- (17) Zamora, A.; Viguera, G.; Rodríguez, V.; Santana, M. D.; Ruiz, J. Cyclometalated Iridium(III) Luminescent Complexes in Therapy and Phototherapy. *Coord. Chem. Rev.* **2018**, *360*, 34–76.

- (18) Stacey, O. J.; Pope, S. J. A. New Avenues in the Design and Potential Application of Metal Complexes for Photodynamic Therapy. *RSC Adv.* **2013**, *3*, 25550–25564.
- (19) Jiang, X.; Zhu, N.; Zhao, D.; Ma, Y. New Cyclometalated Transition-Metal Based Photosensitizers for Singlet Oxygen Generation and Photodynamic Therapy. *Sci. China: Chem.* **2016**, *59*, 40–52.
- (20) Wang, C.; Lystrom, L.; Yin, H.; Hetu, M.; Kilina, S.; McFarland, S. A.; Sun, W. Increasing the Triplet Lifetime and Extending the Ground-State Absorption of Biscyclometalated Ir(III) Complexes for Reverse Saturable Absorption and Photodynamic Therapy Applications. *Dalton Trans.* **2016**, *45*, 16366–16378.
- (21) Li, Y.; Tan, C. P.; Zhang, W.; He, L.; Ji, L. N.; Mao, Z. W. Phosphorescent Iridium(III)-Bis-N-Heterocyclic Carbene Complexes as Mitochondria-Targeted Theranostic and Photodynamic Anticancer Agents. *Biomaterials* **2015**, *39*, 95–104.
- (22) Majumdar, P.; Yuan, X.; Li, S.; Le Guennic, B.; Ma, J.; Zhang, C.; Jacquemin, D.; Zhao, J. Cyclometalated Ir(III) Complexes with Styryl-BODIPY Ligands Showing Near IR Absorption/Emission: Preparation, Study of Photophysical Properties and Application as Photodynamic/Luminescence Imaging Materials. *J. Mater. Chem. B* **2014**, *2*, 2838–2854.
- (23) Chen, Y.; Guan, R.; Zhang, C.; Huang, J.; Ji, L.; Chao, H. Two-Photon Luminescent Metal Complexes for Bioimaging and Cancer Phototherapy. *Coord. Chem. Rev.* **2016**, *310*, 16–40.
- (24) Lo, K. K.-W.; Zhang, K. Y. Iridium(III) Complexes as Therapeutic and Bioimaging Reagents for Cellular Applications. *RSC Adv.* **2012**, *2*, 12069–12083.
- (25) He, L.; Li, Y.; Tan, C.-P.; Ye, R.-R.; Chen, M.-H.; Cao, J.-J.; Ji, L.-N.; Mao, Z.-W. Cyclometalated Iridium(III) Complexes as Lysosome-targeted Photodynamic Anticancer and Real-time Tracking Agents. *Chem. Sci.* **2015**, *6*, 5409–5418.
- (26) Liu, S.; Liang, H.; Zhang, K. Y.; Zhao, Q.; Zhou, X.; Xu, W.; Huang, W. A Multifunctional Phosphorescent Iridium(III) Complex for Specific Nuclear Staining and Hypoxia Monitoring. *Chem. Commun.* **2015**, *51*, 7943–7946.
- (27) Zhang, G.; Zhang, H.; Gao, Y.; Tao, R.; Xin, L.; Yi, J.; Li, F.; Liu, W.; Qiao, J. Near-Infrared-Emitting Iridium(III) Complexes as Phosphorescent Dyes for Live Cell Imaging. *Organometallics* **2014**, *33*, 61–68.
- (28) Lv, W.; Zhang, Z.; Zhang, K. Y.; Zhang, Y.; Yang, H.; Liu, S.; Xu, A.; Guo, S.; Zhao, Q.; Huang, W. A Mitochondria-Targeted Photosensitizer Showing Improved Photodynamic Therapy Effects under Hypoxia. *Angew. Chem., Int. Ed.* **2016**, *55*, 9947–9951.
- (29) Li, S. P.-Y.; Lau, C. T.-S.; Louie, M.-W.; Lam, Y.-W.; Cheng, S. H.; Lo, K. K.-W. Mitochondria-targeting Cyclometalated Iridium(III)-PEG Complexes with Tunable Photodynamic Activity. *Biomaterials* **2013**, *34*, 7519–7532.
- (30) Qiu, K.; Ouyang, M.; Liu, Y.; Huang, H.; Liu, C.; Chen, Y.; Ji, L.; Chao, H. Two-photon Photodynamic Ablation of Tumor Cells by Mitochondria-targeted Iridium(III) Complexes in Aggregated States. *J. Mater. Chem. B* **2017**, *5*, 5488–5498.
- (31) Ouyang, M.; Zeng, L.; Qiu, K.; Chen, Y.; Ji, L.; Chao, H. Cyclometalated Ir^{III} Complexes as Mitochondria-Targeted Photodynamic Anticancer Agents. *Eur. J. Inorg. Chem.* **2017**, *2017*, 1764–1771.
- (32) Zheng, Y.; He, L.; Zhang, D.-Y.; Tan, C.-P.; Ji, L.-N.; Mao, Z.-W. Mixed-ligand Iridium(III) Complexes as Photodynamic Anticancer Agents. *Dalton Trans.* **2017**, *46*, 11395–11407.
- (33) He, L.; Li, Y.; Tan, C.-P.; Ye, R.-R.; Chen, M.-H.; Cao, J.-J.; Ji, L.-N.; Mao, Z.-W. Cyclometalated Iridium(III) Complexes as Lysosome-targeted Photodynamic Anticancer and Real-time Tracking Agents. *Chem. Sci.* **2015**, *6*, 5409–5418.
- (34) Nam, J. S.; Kang, M. G.; Kang, J.; Park, S. Y.; Lee, S. J.; Kim, H. T.; Seo, J. K.; Kwon, O. H.; Lim, M. H.; Rhee, H. W.; Kwon, T. H. Endoplasmic Reticulum-Localized Iridium(III) Complexes as Efficient Photodynamic Therapy Agents via Protein Modifications. *J. Am. Chem. Soc.* **2016**, *138*, 10968–10977.
- (35) Cao, R.; Jia, J.; Ma, X.; Zhou, M.; Fei, H. Membrane Localized Iridium(III) Complexes Induces Endoplasmic Reticulum Stress and Mitochondria-Mediated Apoptosis in Human Cancer Cells. *J. Med. Chem.* **2013**, *56*, 3636–3644.
- (36) Tian, X.; Zhu, Y.; Zhang, M.; Luo, L.; Wu, J.; Zhou, H.; Guan, L.; Battaglia, G.; Tian, Y. Localization Matters: A Nuclear Targeting Two-photon Absorption Iridium Complex in Photodynamic Therapy. *Chem. Commun.* **2017**, *53*, 3303–3306.
- (37) Wilkinson, A. J.; Puschmann, H.; Howard, J. A. K.; Foster, C. E.; Williams, J. A. G. Luminescent Complexes of Iridium(III) Containing N^CN-Coordinating Tridentate Ligands. *Inorg. Chem.* **2006**, *45*, 8685–8699.
- (38) Williams, J. A. G.; Wilkinson, A. J.; Whittle, V. L. Light-Emitting Iridium Complexes with Tridentate Ligands. *Dalton Trans.* **2008**, 2081–2099.
- (39) Liu, B.; Monro, S.; Lystrom, L.; Cameron, C. G.; Colon, K.; Yin, H.; Kilina, S.; McFarland, S. A.; Sun, W. Photophysical and Photobiological Properties of Dinuclear Iridium(III) Bis-tridentate Complexes. *Inorg. Chem.* **2018**, *57*, 9859–9872.
- (40) Collin, J.-P.; Dixon, I. M.; Sauvage, J.-P.; Williams, J. A. G.; Barigelletti, F.; Flamigni, L. Synthesis and Photophysical Properties of Iridium(III) Bis(terpyridine) and Its Homologues: A Family of Complexes with a Long-Lived Excited State. *J. Am. Chem. Soc.* **1999**, *121*, 5009–5016.
- (41) Goldstein, D. C.; Cheng, Y. Y.; Schmidt, T. W.; Bhadbhade, M.; Thordarson, P. Photophysical Properties of a New Series of Water Soluble Iridium Bis(terpyridine) Complexes Functionalised at the 4' Position. *Dalton Trans.* **2011**, *40*, 2053–2061.
- (42) Leslie, W.; Batsanov, A. S.; Howard, J. A. K.; Williams, J. A. G. Cross-couplings in the elaboration of luminescent bis-terpyridyl iridium complexes: the effect of extended or inhibited conjugation on emission. *Dalton Trans.* **2004**, 623–631.
- (43) Kam-Wing Lo, K.; Chung, C.-K.; Chun-Ming Ng, D.; Zhu, N. Syntheses, characterisation and photophysical studies of novel biological labelling reagents derived from luminescent iridium(III) terpyridine complexes. *New J. Chem.* **2002**, *26*, 81–88.
- (44) Cavazzini, M.; Quici, S.; Scalera, C.; Puntoriero, F.; La Ganga, G.; Campagna, S. Synthesis, Characterization, Absorption Spectra, and Luminescence Properties of Multinuclear Species Made of Ru(II) and Ir(III) Chromophores. *Inorg. Chem.* **2009**, *48*, 8578–8592.
- (45) Hvasanov, D.; Mason, A. F.; Goldstein, D. C.; Bhadbhade, M.; Thordarson, P. Optimising the synthesis, polymer membrane encapsulation and photoreduction performance of Ru(II)- and Ir(III)-bis(terpyridine) cytochrome c bioconjugates. *Org. Biomol. Chem.* **2013**, *11*, 4602–4612.
- (46) Jacques, A.; Kirsch-De Mesmaeker, A.; Elias, B. Selective DNA Purine Base Photooxidation by Bis-terdentate Iridium(III) Polypyridyl and Cyclometalated Complexes. *Inorg. Chem.* **2014**, *53*, 1507–1512.
- (47) Matias, T. A.; Mangoni, A. P.; Toma, S. H.; Rein, F. N.; Rocha, R. C.; Toma, H. E.; Araki, K. Catalytic Water-Oxidation Activity of a Weakly Coupled Binuclear Ruthenium Polypyridyl Complex. *Eur. J. Inorg. Chem.* **2016**, *2016*, 5547–5556.
- (48) Barbour, J. C.; Kim, A. J. I.; DeVries, E.; Shaner, S. E.; Lovaasen, B. M. Chromium(III) Bis-Arylterpyridyl Complexes with Enhanced Visible Absorption via Incorporation of Intraligand Charge-Transfer Transitions. *Inorg. Chem.* **2017**, *56*, 8212–8222.
- (49) Peng, X.; Xu, Y.; Sun, S.; Wu, Y.; Fan, J. A Ratiometric Fluorescent Sensor for Phosphates: Zn²⁺-Enhanced ICT and Ligand Competition. *Org. Biomol. Chem.* **2007**, *5*, 226–228.
- (50) Jung, H. S.; Han, J.; Shi, H.; Koo, S.; Singh, H.; Kim, H. J.; Sessler, J. L.; Lee, J. Y.; Kim, J. H.; Kim, J. S. Overcoming the Limits of Hypoxia in Photodynamic Therapy: A Carbonic Anhydrase IX-Targeted Approach. *J. Am. Chem. Soc.* **2017**, *139*, 7595–7602.
- (51) Chirdon, D. N.; Transue, W. J.; Kagalwala, H. N.; Kaur, A.; Maurer, A. B.; Pintauer, T.; Bernhard, S. [Ir(N^CN)(C^N)L]⁺: A New Family of Luminophores Combining Tunability and Enhanced Photostability. *Inorg. Chem.* **2014**, *53*, 1487–1499.

- (52) Melhuish, W. H. Quantum Efficiencies of Fluorescence of Organic Substances: Effect of Solvent and Concentration of the Fluorescent Solute. *J. Phys. Chem.* **1961**, *65*, 229–235.
- (53) Suzuki, K.; Kobayashi, A.; Kaneko, S.; Takehira, K.; Yoshihara, T.; Ishida, H.; Shiina, Y.; Oishi, S.; Tobita, S. Reevaluation of Absolute Luminescence Quantum Yields of Standard Solutions Using a Spectrometer with an Integrating Sphere and a Back-Thinned CCD Detector. *Phys. Chem. Chem. Phys.* **2009**, *11*, 9850–9860.
- (54) Carmichael, I.; Hug, G. L. Triplet-Triplet Absorption Spectra of Organic Molecules in Condensed Phases. *J. Phys. Chem. Ref. Data* **1986**, *15*, 1–250.
- (55) Kumar, C. V.; Qin, L.; Das, P. K. Aromatic Thioketone Triplets and Their Quenching Behaviour towards Oxygen and Di-*t*-Butylnitroxyl Radical. A Laser-Flash-Photolysis Study. *J. Chem. Soc., Faraday Trans. 2* **1984**, *80*, 783–793.
- (56) Firey, P. A.; Ford, W. E.; Sounik, J. R.; Kenney, M. E.; Rodgers, M. A. J. Silicon Naphthalocyanine Triplet State and Oxygen. A Reversible Energy-Transfer Reaction. *J. Am. Chem. Soc.* **1988**, *110*, 7626–7630.
- (57) DeRosa, M. C.; Crutchley, R. J. Photosensitized Singlet Oxygen and Its Applications. *Coord. Chem. Rev.* **2002**, *233–234*, 351–371.
- (58) Kohn, W.; Sham, L. J. Self-Consistent Equations Including Exchange and Correlation Effects. *Phys. Rev.* **1965**, *140*, A1133–A1138.
- (59) Frisch, M. J.; Trucks, G. W.; Schlegel, H. B.; Scuseria, G. E.; Robb, M. A.; Cheeseman, J. R.; Scalmani, G.; Barone, V.; Petersson, G. A.; Nakatsuji, H.; Li, X.; Caricato, M.; Marenich, A. V.; Bloino, J.; Janesko, B. G.; Gomperts, R.; Mennucci, B.; Hratchian, H. P.; Ortiz, J. V.; Izmaylov, A. F.; Sonnenberg, J. L.; Williams-Young, D.; Ding, F.; Lipparini, F.; Egidi, F.; Goings, J.; Peng, B.; Petrone, A.; Henderson, T.; Ranasinghe, D.; Zakrzewski, V. G.; Gao, J.; Rega, N.; Zheng, G.; Liang, W.; Hada, M.; Ehara, M.; Toyota, K.; Fukuda, R.; Hasegawa, J.; Ishida, M.; Nakajima, T.; Honda, Y.; Kitao, O.; Nakai, H.; Vreven, T.; Throssell, K.; Montgomery, J. A., Jr.; Peralta, J. E.; Ogliaro, F.; Bearpark, M. J.; Heyd, J. J.; Brothers, E. N.; Kudin, K. N.; Staroverov, V. N.; Keith, T. A.; Kobayashi, R.; Normand, J.; Raghavachari, K.; Rendell, A. P.; Burant, J. C.; Iyengar, S. S.; Tomasi, J.; Cossi, M.; Millam, J. M.; Klene, M.; Adamo, C.; Cammi, R.; Ochterski, J. W.; Martin, R. L.; Morokuma, K.; Farkas, O.; Foresman, J. B.; Fox, D. J. *Gaussian16*, Revision B.01; Gaussian, Inc.: Wallingford, CT, 2016.
- (60) Gill, P. M. W.; Johnson, B. G.; Pople, J. A.; Frisch, M. J. The performance of the Becke-Lee-Yang-Parr (B-LYP) density functional theory with various basis sets. *Chem. Phys. Lett.* **1992**, *197*, 499–505.
- (61) Hay, P. J.; Wadt, W. R. Ab initio effective core potentials for molecular calculations. Potentials for the transition metal atoms Sc to Hg. *J. Chem. Phys.* **1985**, *82*, 270–283.
- (62) Clark, T.; Chandrasekhar, J.; Spitznagel, G. W.; Schleyer, P. V. R. Efficient diffuse function-augmented basis sets for anion calculations. III. The 3-21+G basis set for first-row elements, Li–F. *J. Comput. Chem.* **1983**, *4*, 294–301.
- (63) Barone, V.; Cossi, M.; Tomasi, J. Geometry optimization of molecular structures in solution by the polarizable continuum model. *J. Comput. Chem.* **1998**, *19*, 404–417.
- (64) Casida, M. E.; Jamorski, C.; Casida, K. C.; Salahub, D. R. Molecular excitation energies to high-lying bound states from time-dependent density-functional response theory: Characterization and correction of the time-dependent local density approximation ionization threshold. *J. Chem. Phys.* **1998**, *108*, 4439–4449.
- (65) Martin, R. L. Natural transition orbitals. *J. Chem. Phys.* **2003**, *118*, 4775–4777.
- (66) Humphrey, W.; Dalke, A.; Schulten, K. VMD: Visual molecular dynamics. *J. Mol. Graphics* **1996**, *14*, 33–38.
- (67) Michalec, J. F.; Bejune, S. A.; Cuttall, D. G.; Summerton, G. C.; Gertenbach, J. A.; Field, J. S.; Haines, R. J.; McMillin, D. R. Long-Lived Emissions from 4'-Substituted Pt(Tryp)Cl⁺ Complexes Bearing Aryl Groups. Influence of Orbital Parentage. *Inorg. Chem.* **2001**, *40*, 2193–2200.
- (68) Ji, Z.; Li, S.; Li, Y.; Sun, W. Back-to-back dinuclear platinum terpyridyl complexes: Synthesis and photophysical studies. *Inorg. Chem.* **2010**, *49*, 1337–1346.
- (69) Maity, D.; Das, S.; Mardanya, S.; Baitalik, S. Synthesis, Structural Characterization, and Photophysical, Spectroelectrochemical, and Anion-Sensing Studies of Heteroleptic Ruthenium(II) Complexes Derived from 4'-Polyaromatic-Substituted Terpyridine Derivatives and 2,6-Bis(Benzimidazol-2-Yl)Pyridine. *Inorg. Chem.* **2013**, *52*, 6820–6838.
- (70) Guo, F.; Sun, W. Photophysics and Optical Limiting of Platinum(II) 4'-Arylterpyridyl Phenylacetylde Complexes. *J. Phys. Chem. B* **2006**, *110*, 15029–15036.
- (71) Liu, R.; Dandu, N.; Li, Y.; Kilina, S.; Sun, W. Synthesis, Photophysics and Reverse Saturable Absorption of Bipyridyl Platinum(II) Bis(arylfluorenylacetylde) Complexes. *Dalton Trans.* **2013**, *42*, 4398–4409.
- (72) Ogilby, P. R.; Foote, C. S. Chemistry of Singlet Oxygen. 42. Effect of Solvent, Solvent Isotopic Substitution, and Temperature on the Lifetime of Singlet Molecular Oxygen (¹Δ_g). *J. Am. Chem. Soc.* **1983**, *105*, 3423–3430.
- (73) O'Brien, J.; Wilson, I.; Orton, T.; Pognan, F. Investigation of the Alamar Blue (resazurin) Fluorescent Dye for the Assessment of Mammalian Cell Cytotoxicity. *Eur. J. Biochem.* **2000**, *267*, 5421–5426.
- (74) Daghestanli, N. A.; Itri, R.; Baptista, M. S. Singlet Oxygen Reacts with 2',7'-Dichlorodihydrofluorescein and Contributes to the Formation of 2',7'-Dichlorofluorescein. *Photochem. Photobiol.* **2008**, *84*, 1238–1243.